Article

Functional avidity of anti-B7H3 CAR-T constructs predicts antigen density thresholds for triggering effector function

Marta Barisa [1] ✉, Henrike P. Muller [1,8], Elisa Zappa[2,8], Rivani Shah[1], Juliane L. Buhl[2,3], Benjamin Draper[1], Courtney Himsworth [1], Chantelle Bowers[1], Sophie Munnings-Tomes[1], Marilena Nicolaidou [1], Sonia Morlando[1], Kathleen Birley[1], Clara Leboreiro-Babe [1], Alice Vitali[1], Laura Privitera[1], Kyle O'Sullivan[1], Ailsa Greppi[1], Magdalena Buschhaus[4], Mario Barrera Román [2,3], Sam de Blank [2,3], Femke van den Ham[2], Brenna R. van 't Veld[2], Gabrielle Ferry[1], Jonathan Fisher [1], Debarati Shome[4], Reza Nadafi[4], Israrul H. Ansari[5], Rogier Reijmers [4], Stefano Giuliani[1], Paul Sondel[5], Laura K. Donovan [1], Louis Chesler [6], Jan Molenaar[2], Jarno Drost [2,3], Anne C. Rios [2,3], Kerry Chester [7], Judith Wienke [2] ✉ & John Anderson [1] ✉

Chimeric Antigen receptor T cell (CAR-T) treatments for solid cancers have been compromised by limited expansion and survival in the tumor microenvironment following interaction with antigen-expressing target cells. Using B7H3 as a model antigen with broad clinical applicability, we evaluate the relationship between the antibody/antigen affinity of three clinical candidate binders and the three following characteristics: cellular avidity, duration of sustained cytotoxicity in tumoroid re-stimulation assays, and in vivo anti-tumoral responses. Next, BEHAV3D video microscopy is used to assess CAR-T cell interaction with tumor cells at single cell resolution. These data are consistent with a threshold avidity of CAR-T / tumor cell interaction and target cell B7H3 expression level, where enhanced functionality is characterized by longer cumulative CD8+ CAR-T / tumor target interaction times, CAR-T cell expansion and sustained tumor control. Lower checkpoint receptor expression does not correlate with enhanced anti-tumor function. These results provide further insights into design of anti-B7H3 CAR-T cells for antigen-dim cell targeting, and avoidance of antigen-dim tumor relapse.

Genetic modification of a cancer patients' T cells with Chimeric antigen receptors (CAR-T cells) for adoptive transfer immunotherapy is a rapidly expanding clinical and scientific field. Clinical studies targeting hematological malignancies using adoptively-transferred CAR-T cell therapy have resulted in FDA approvals of CAR-T products for the treatment of leukemia, lymphoma, and myeloma. In contrast, far fewer durable clinical responses attributable to CAR-T cells are reported in solid cancers despite considerable efforts[1]. A major reason for the relative failure of CAR-T cell adoptive transfer in the solid cancer setting is suboptimal T cell functionality, evidenced by a lack of T cell proliferation and persistence. Reasons for this failure can likely be distilled down to inhibitory effects of the tumor microenvironment

and inherent failure of CARs to provide optimal signals to the T cell upon target engagement[2,3].

CARs comprise an antigen-sensing ectodomain, which is typically a single chain variable fragment (scFv) of an antibody, and endodomains that are an amalgamation of ITAM-containing T cell receptor (TCR) signaling domains, most typically the ζ-chain of CD3, and co-stimulatory domains. CAR-T cells thereby commandeer the MHC-unrestricted antigen specificity of a monoclonal antibody and combine it with T cell signaling in a single molecule. The triggering of T cell activity is dependent on the formation of an effective immune synapse with an antigen-positive target cell. Once a productive synapse is formed, signaling occurs through engagement of the CD3ζ and co-stimulatory moieties with proximal signaling molecules, leading to T cell effector functions and a pro-inflammatory response.

For example, structural features of the CAR that influence persistence of effector function include hinge and transmembrane components, and choice and orientation of co-stimulatory endodomains. Moreover, certain scFv binders that signal in the absence of antigen contribute to excessive signaling and subsequent T cell dysfunction[4,5]. Studies in CD19-expressing leukemia have shown that scFv affinity can affect the strength and duration of the immune synapse with consequences for subsequent disease control[6]. The quality and quantity of immune synapse formation are influenced by binder affinity (both on- and off-rate), target antigen density and CAR expression density. Cellular avidity (strength of association between a CAR-T cell and its cellular target), is similarly governed by both affinity of interaction and expression levels of CAR and antigen in the interacting cells. A detailed understanding is lacking regarding optimal CAR scFv for solid tumor-targeting CAR-T cells, and how scFv affinity and avidity impact sustained functionality in solid tumors.

To address these challenges, we chose a broadly expressed solid tumor cancer antigen that is targeted in a number of current CAR-T clinical studies in solid tumors. B7H3 is expressed on solid and hematological cancers in the adult and pediatric settings[7,8]. A member of the immunoglobulin superfamily and closely related to PD-L1, B7H3 is enriched on high-grade tumors and expressed at low levels on healthy tissue[9–14]. There are several B7H3 binders that have been or are being progressed to evaluation in clinical trials, including MGA271, 376.96 and TE9[8,10,15]. To specifically evaluate the impact of the scFv binding properties on CAR-T function, we cloned these three different binders into identical viral backbones. All constructs had a second-generation 28ζ endodomain and CD8 hinge and transmembrane format, and hence we set out to determine generalizable relationships between binder properties with CAR-T function rather than evaluate the binders in the context of their optimized formats for clinical studies.

Many studies have demonstrated avidity to affect CAR-T function[16–18]. Contrary to the expectations based on some preceding literature[6,19–21], we observe that CAR-T incorporating either of two scFv's that form high avidity interactions with B7H3-expressing cells, mediate superior anti-tumor functionality compared to a low avidity scFv, a result concordant with other previously published results[22]. Both high and low avidity interactions enable acute cytotoxicity and cytokine production, but only high avidity interactions lead to sustained CAR-T proliferation and consequent activity in the re-challenge setting. These differences in scFv-driven functional potential are most evident against B7H3[med] or B7H3[dim] targets, the consequence of which is the emergence of antigen-dim escape variants with the low avidity binder. We postulate that, in order to mediate tumor control, B7H3 CAR-T cells need to interact with their target cell with a supra-threshold avidity, sufficient to drive initial activation and proliferation.

Results

MGA271, 376.96, and TE9 scFv CAR-T cells mediate divergent responses against in vivo models of solid tumors

MGA271[23], 376.98[24], and TE9[25] scFv's were cloned into a CD8-28ζ second-generation CAR format containing a CD8α hinge-transmembrane, and expressed in SFG γ-retroviral vector with an EF1α promoter as described previously[25,26]. A compact epitope tag, RQR8[27], was co-expressed from the construct to monitor CAR-T transduction efficiency (Fig. 1a). Transgene co-expression between the binders was validated by staining the CAR directly with B7H3-His protein (Supplementary Fig. 1). Against LAN-1 and Kelly neuroblastoma targets, we generally observed enhanced CAR-T cytokine production for 28ζ compared to 4-1BBζ endodomain for all three binders, consistent with previous literature including our own data[8,25,28], and which correlated with higher exhaustion/activation marker expression (Supplementary Fig. 2). CD28 costimulation was, therefore, chosen over 4-1BB.
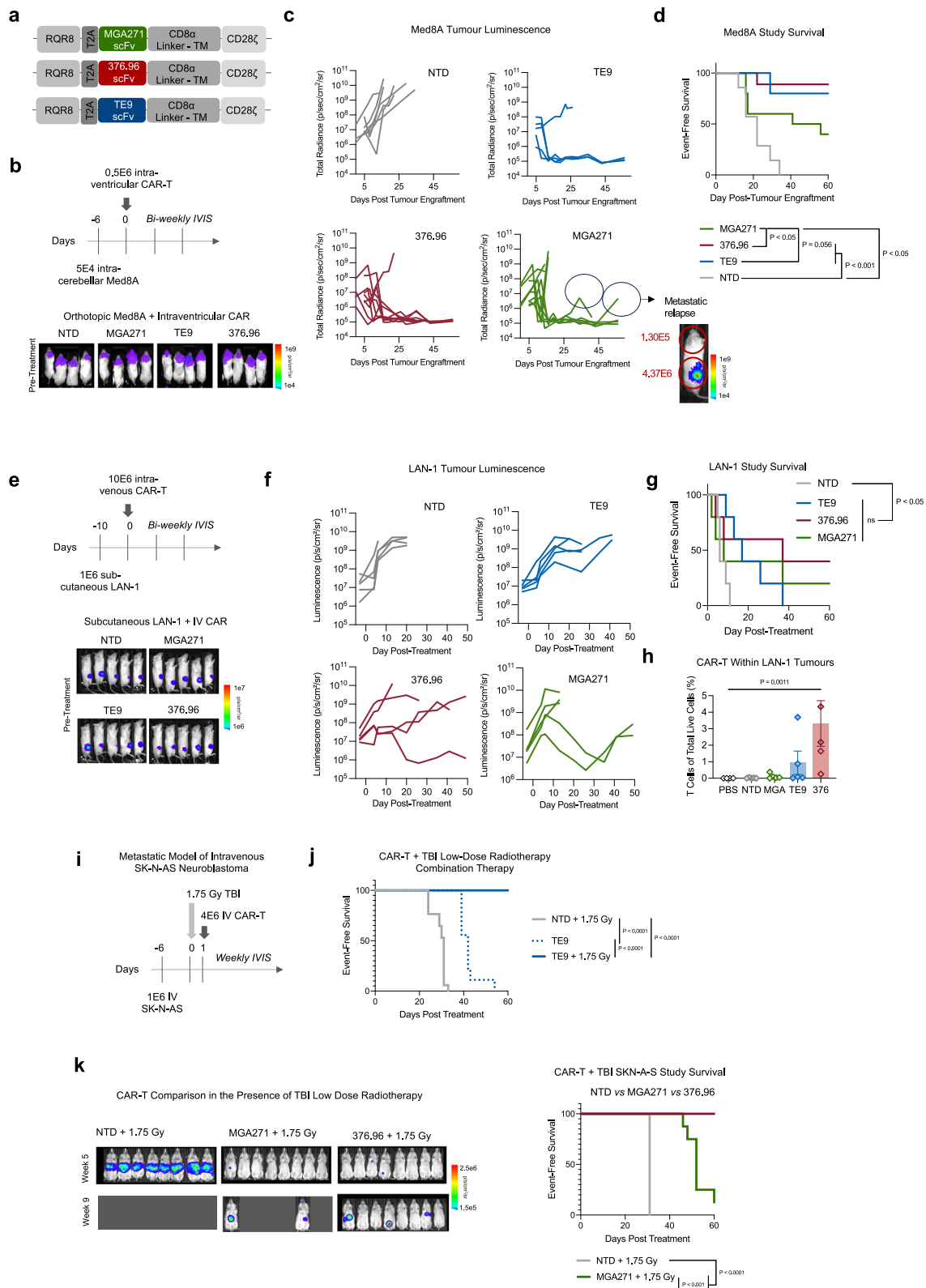
We evaluated CAR-T in vivo performance in an orthotopic, B7H3-positive[29] Med8A model of medulloblastoma in which NOD.Cg-Prkdc scid Il2rg tm1Wjl /SzJ (NSG) mice received intraventricular CAR-T cells after cerebellar tumor engraftment (Fig. 1b). This treatment regimen of 0.5×10^6 CAR-T six days following tumor engraftment ("high-stress" model) was chosen to discriminate CAR-T function since treatment with 2.5×10^6 TE9 CAR-T two days following tumor engraftment ("low-stress" model) had generated a 100% cure-rate (Supplementary Fig. 3a). While all three CAR constructs enhanced animal survival over untreated or non-transduced (NTD) T cells (Supplementary Fig. 3b), TE9-28ζ and 376.96-28ζ treatments outperformed MGA271-28ζ, including in the prevention of metastatic relapse (Fig. 1c, d). Tumors were harvested to evaluate CAR-T cell persistence, but the viability of the collected and largely necrotic tissue was too poor to robustly compare CAR-T intratumoral persistence.

We have previously shown that MGA271, 376.96 and TE9-28ζ scFv CAR-T are equivalent in short-term single challenge cytotoxicity assays against LAN-1 neuroblastoma cells, and that TE9-28ζ CAR-T enhanced survival in a difficult-to-treat subcutaneous LAN-1 NSG model[25]. We, therefore, evaluated MGA271 and 376.96-28ζ CAR-T in the same vivo model (illustrated in Fig. 1e). In contrast with the Med8A model where differences between binders were evident, all CAR-T constructs performed similarly against LAN-1 tumors and failed to effect consistent cures (Fig. 1f, g and Supplementary Fig. 4a). Viable subcutaneous tumors could, however, be extracted from animals at cull, whereby mice treated with 376.96 and TE9 CAR-T contained more detectable human T cells than those treated with PBS, non-transduced T cells or MGA271-CARs (Fig. 1h).

CAR-T efficacy in the neuroblastoma setting was then evaluated in an intravenously-infused metastatic SKN-A-S model (Fig. 1i and Supplementary Fig. 4b). Similar to the LAN-1 model, anti-B7H3 CAR-T monotherapy (in the form of TE9) was only marginally efficacious against tumors (Fig. 1j). However, TE9 CAR-T efficacy in this model could be vastly enhanced by adding low dose (1.75 Gy) total body irradiation, administered one day prior to CAR-T infusion (Fig. 1i, j and Supplementary Fig. 4c). In a separate study using this protocol, 376.96 CAR-T protected animals from death by metastatic disease burden over a 60-day study period, while MGA271 and NTD CAR-T cells did not (Fig. 1k). Taken together, these in vivo models establish that B7H3 CAR-T functionality can be affected by scFv selection, but in a manner that is dependent on the tumor model.

MGA271 CAR-T have a lower avidity than 376.96 and TE9 CAR-T for B7H3-expressing tumor cells

Despite achieving similar high transduction efficiencies with all three binder CARs (Supplementary Fig. 1), we noted that MGA271 CAR-T staining with B7H3-his protein was dimmer than that of matched 376.96 and TE9 CAR-T (Fig. 2a–c and Supplementary Fig. 5a, b). The

same was true when comparing MGA271 and TE9 CAR staining with Protein L (Fig. 2c).

Using the Earth Mover's Distance algorithm[30], we quantified expression of CAR-T relative to non-transduced T cells with anti-RQR8, B7H3-his, anti-Fab or Protein L, in which anti-RQR8 serves as control for vector transcriptional strength whilst B7H3-his determines binding to target antigen, and Protein L/anti-Fab represent

expression of respective CARs (Fig. 2d). Binders TE9 and 376.96 bound equivalent amounts of B7H3 protein and anti-Fab, indicating a matched degree of antigen binding as well as CAR expression (Supplementary Fig. 5c, d). In contrast, MGA271 had weaker binding to B7H3-his than TE9 and 376 (Supplementary Fig. 5c) and lower expression than TE9 as disclosed by Protein L staining (Supplementary Fig. 5e). Taken together, the data suggest this MGA271-

Fig. 1 | MGA271, 376.96 and TE9 scFv's mediate divergent CAR-T responses against in vivo models of medulloblastoma and neuroblastoma. a Schematic of the SFG backbone retroviral constructs. **b** Schematic of orthotopic, luciferase+ Med8A medulloblastoma tumor model in NSG mice with representative pre-treatment images. The experiment was repeated twice; each treatment group is representative of at least $N = 5$ animals. **c** Serial tumor luminescence measurements including at instances of metastatic relapse. **d** Event (acute tumor burden toxicity)-free survival was compared between the different T cell treatment groups (Log-Rank Mantel−Cox Test 376 x MGA $p = 0.018$; TE9 x MGA $p = 0.056$). **e** Representative pre-treatment images of luciferase+ LAN-1 neuroblastoma tumor model in NSG mice ($N = 5$). **f** Serial tumor luminescence measurements for all animals. **g** Event (tumors exceeding permissible 1×10^9 p/s/cm²/sr threshold prior to cull on ethical grounds)-free survival (log-rank Mantel−Cox test 376 x NT $p = 0.0051$; TE9 x NT $p = 0.0053$; MGA x NT $p = 0.0296$). **h** Tumors from LAN-1-engrafted animals were collected at cull and processed for flow cytometric analysis to assess live human T cell content of total live cells within the tumor mass (error bars ± SEM, $N = 5$; Kruskal−Wallis test). **i** Schematic of metastatic, luciferase+ SKN-A-S neuroblastoma tumor model in NSG mice. **j** SKN-A-S model: event (acute toxicity from tumor burden)-free survival of non-transduced or TE9 CAR-T cell treatment combined with 1.75 Gy total body irradiation (TBI) ($N = 9$; log-rank Mantel−Cox test). **k** Preliminary data from a single experiment of SKN-A-S treatment with 1.75. Gy TBI and MGA271 or 376.96 binder-CAR-T cells. Representative luminescence data over time on the left, and event (acute toxicity from tumor burden)-free survival comparison on the right: 8−9 animals per group; comparisons using a log-rank Mantel−Cox test.

containing CAR has lower surface expression reflecting weaker cell staining with the antigenic target.

We further hypothesized that the second contributing factor may be the strength of the different scFvs' binding to the B7H3 protein. The on- and off-rates for each binder in IgG1 format for 4-Ig B7H3 were measured using Biacore Surface Plasmon Resonance (Fig. 2e, f and Supplementary Fig. 5f). TE9 had the highest affinity for B7H3 (0.44 nM), similar to 376.96 (0.69 mM), with both being higher than MGA271 (1.61 nM). It was of interest that TE9 had both the highest on-rate and the highest off-rate, whilst 376.9 had relatively slow on- and off-rates; hence, dissociation constant (K_D) values of TE9 and 376.9 were similar (Fig. 2g). Binder affinity for B7H3 correlated with the intensity of staining of CAR-T cells with recombinant B7H3-his protein (Fig. 2h).

Thus, we hypothesized that the differential CAR expression at the cell surface, combined with different affinity for target antigen, may impact the strength of the immune synapse between CAR-T and antigen-positive target cells, and that this may, moreover, correlate with the differences observed between the binders in the in vivo studies. To test this, we evaluated the strength of the cell-to-cell interaction for each of these CAR-T cells with cell lines representing a range of antigen expression (Fig. 2i). To avoid differences in transduction efficiency biasing avidity measurement, CAR-T of all scFv's were diluted with donor-matched NTD T cells to standardize expression of the RQR8 marker gene (Supplementary Fig. 5g). Avidity measurements were made using a Lumicks z-Movi Cell Avidity Analyzer, which measures the force (in piconewtons, pN) required to detach a population of effector cells from their targets (Fig. 2j). None of the CAR-T bound B7H3^neg SupT1-WT cells, whilst all three bound B7H3^pos cells, albeit with different avidities (Fig. 2k−m). TE9 and 376.96 scFv CAR-T consistently bound antigen-positive target cells with higher avidity than MGA271 or NTD cells.

Target cells with high B7H3 per cell overall formed higher avidity interactions with CAR-T, although the positive correlation between binding strength and antigen density was more pronounced for TE9 and 376.96 than MGA271 (Fig. 2m). This suggested that the strength of the B7H3 CAR immune synapse is driven by three factors: the level of CAR expression at the T cell surface, the affinity of the scFv for B7H3 and the B7H3 density on target cells. We then sought to evaluate how this impacts CAR function mechanistically.
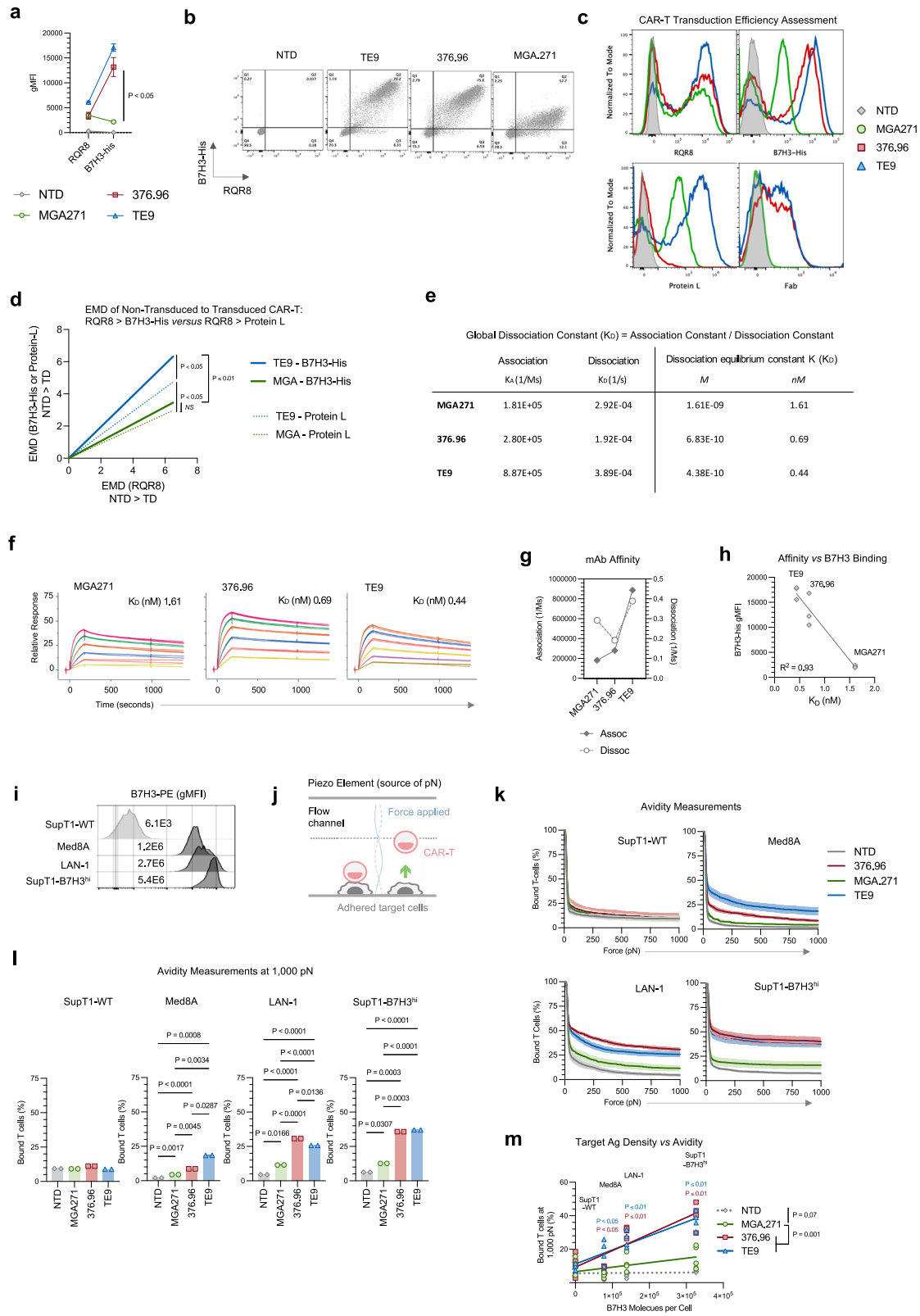
Cytotoxic capacity of low-avidity MGA271 CAR-T deteriorates upon rechallenges with B7H3^dim tumors

To examine the impact of CAR-T binding avidity on effector function, the different constructs were assessed against solid tumor target cells that express a range of B7H3 densities. We selected five different B7H3^pos target types, which were either cell lines or primary neurosphere cultures (defined hereafter as "tumoroids"), derived from pediatric solid tumors with a broad range of B7H3 antigen densities as determined using QuantiBright beads (Fig. 3a).

CAR-T cytotoxicity was first evaluated at a range of E:T ratios in single-challenge short-term (4 h) assays. All binders displayed equivalent effective cytotoxicity against B7H3^hi neuroblastoma cell lines LAN-1 and Kelly at relatively high E:T ratios ranging from 10:1 to 1.25:1 (Fig. 3b), but this equivalence was lost in longer timecourse assays (72 h) as the E:T ratios were decreased further (Fig. 3c). Similar relative failure of the lower avidity MGA271 binder was seen when targeting the lower B7H3 antigen density neuroblastoma tumoroids at low E:T ratios (≤1:10) (Fig. 3d).

The capacity of CAR-T constructs to maintain killing on repeat encounters with target cells is essential for their clinical utility. Therefore, CAR-T were re-challenged over a four-week co-culture as illustrated in Fig. 3e. Allowing the CAR-T cells one week to effect cytotoxicity, 691-T tumoroids were killed by both low-avidity CAR MGA271 and high avidity 376.96 and TE9 CAR-T following the first challenge (Fig. 3f). However, MGA271 killing dropped drastically after re-challenge, and by the third challenge, no MGA271-mediated 691-T killing was observed, while higher avidity CAR-T maintained cytotoxicity on rechallenge. Using 691-B tumoroids, which have lower antigen density, the high avidity binders 376.96 and TE9 completely eliminated targets after a single challenge, whilst MGA271 showed no cytotoxicity. All CAR constructs failed against 691-B upon re-challenge (Fig. 3f). A similar trend was observed for B7H3^med 103-T malignant rhabdoid tumoroids (MRT). All CARs were cytotoxic against 103-T, but the inferiority of MGA271 was the most pronounced upon challenge during the third and final week (Fig. 3g, h).

Potential explanations for CAR-T failure in repeat stimulation assays are T cell exhaustion or differentiation to terminal effector cells. We identified upregulation of exhaustion/activation markers on all scFv CAR-T cells following challenge with neuroblastoma targets (Supplementary Fig. 2 for Kelly and LAN-1 cell lines; Supplementary Fig. 6 for 691 tumoroids). We then carried out multi-parametric dimensionality reduction analysis of these flow data on CAR-T cells in the long-term re-challenge assays for which the patient-derived tumoroid cytotoxicity data is shown in Fig. 3f. MGA271 CAR-T clustered separately from TE9 and 376.96 CAR-T following more than one challenge with either 691-B or 691-T target cells, whereby MGA271 CAR-T expressed lower levels of exhaustion/ activation markers PD-1 and TIM-3 as well as concurrently lower levels of CD25 and CD69 (Fig. 3i and Supplementary Fig. 6). This was not the case for CAR-T cells of any species that were not exposed to tumor targets nor matched, non-transduced T cell controls, which clustered closely (Fig. 3i). Relative to tumor-exposed CAR-T, non-transduced and CAR alone control T cells were enriched for CD4⁺ (as opposed to CD8⁺) T cells, CCR7 expression and a naïve (CD45RA⁺CCR7⁺) phenotype (Fig. 3i and Supplementary Fig. 6). Interestingly, TE9 and 376.96 CAR-T memory and exhaustion/activation marker expression following more than one challenge with targets was similar with both 691-B and 691-T tumoroids, even though 691-T cocultures were associated with substantially higher ongoing CAR-T killing. This suggests that T cell signaling was

active and ongoing in the presence of 691-B neuroblastoma, even if cytotoxicity and T cell proliferation were diminished. Overall, the observation that high avidity CAR-T cells exhibited both continuous cytotoxicity as well as expressed higher levels of exhaustion/activation markers, does not support the hypothesis that the expression of markers like PD-1, TIM-3 or LAG-3 is predictive of handicapped performance in the face of repeated, intense challenge with tumor targets.

Rather, expression of these markers was associated with ongoing, CAR-mediated signaling which, in the presence of sufficient target antigen density, can mediate cytotoxic effector function.

Collating data from the tumoroid cocultures at 1:10 E:T ratio, the differences in cytotoxicity between binders at low antigen density was pronounced at both initial challenge and re-challenges, and is represented graphically in Fig. 3j. At the lowest antigen density (~1000

Fig. 2 | 376.96 and TE9 but not MGA271 CAR-T form high avidity interactions with tumor cells in a B7H3 density-dependent manner. a, b Cryopreserved, thawed CAR-T cell surface transgene expression was measured using flow cytometry with clone QBEND10 mAb to detect RQR8 marker gene and histidine-x6 tagged B7H3 protein (B7H3-his) + anti-his mAb to detect the CAR (mean ± SEM, $N = 3$ donors, two-way ANOVA MGA versus 376.98 $p = 0.0257$ MGA versus TE9 $P = 0.0026$). Representative dot plots of gated live (CD3⁺) T cells from one donor shown in (**b**). **c** CAR-T cells stained with Protein L (binds κ light chain) or anti-murine Fab. Representative histograms from one donor gated on live (CD3⁺) T cells. Binder 376.96 (λ-light chain) is noninformative with protein L staining and MGA271 (humanized framework) is noninformative for anti-mouse Fab. **d** Relative cell surface expression of RQR8 and CAR was compared between TE9 and MGA271 CAR-T cells using Earth Mover's Distance (EMD) analysis of the flow cytometry data for RQR8, B7H3-his and Protein L. RQR8 was used as a marker of overall transduction whilst B7H3-his is marker of CAR binding to B7H3; Protein L is marker of CAR surface expression, and EMD measured transduced T cell staining compared to donor-matched non-transduced T cells. Marker expression was compared across three independent T cell donors, and statistical comparison done across linear

regression curve slopes using Dunnett's T3 Multiple Comparisons test (TE9 B7-his vs MGA B7-his $p = 0.0115$, TE9 B7-his vs TE9-pL $p = 0.0054$, TE9-pL vs MGA-pL $p = 0.0235$). Individual donor EMD data were in Supplementary Fig. 5c–e. **e, f** Binder affinity for B7H3 (4-Ig) using whole antibodies in IgG1 format, using Biacore Surface Plasmon Resonance (SPR). **g** Association ("on-rate") and dissociation ("off-rate") rate constants. **h** Binder affinity plotted against the gMFI of B7H3-his protein staining of three independent donor CAR-T cell products. **i** Respective geometric mean fluorescence intensities (gMFI) of B7H3-PE staining of a range of target cells. **j** Principle of Lumicks z-Movi synapse avidity measurement platform. **k** CAR-T detachment plotted against force in pN applied to the T cell/target interaction. Line indicates mean T cell attachment of four independent donors across three experimental replicates with matched donors compared for each construct: shaded area represents SEM. **l** Avidity as represented by attachment at 1000 pN applied force: $N = 4$ donors, each with three experimental replicates, one-way ANOVA. **m** Bound CAR-T (%) at 1000 pN plotted against QuantiBright defined B7H3 molecules per cell. The lines are linear regressions of the means of four individual donors (two-way ANOVA).

molecules per cell for 691-B tumoroids), only the high avidity binders, TE9 and 376.96, were capable of initiating killing at first challenge but failed to sustain cytotoxicity at re-challenge. At ~5000 molecules per cell or more, all the binders were effective at initial challenge, but only the two high-avidity binders sustained killing over multiple rounds of stimulation (Fig. 3j).

The data prompted us to hypothesize that at high antigen density, binders perform similarly because CAR-T signaling for all of them exceeds a threshold for proliferation and cytokine secretion to initiate tumor control. At low antigen density, high avidity interaction is required to exceed this threshold. Therefore, we next evaluated CAR-T effector functions other than cytotoxicity, including IL-2 and IFN-γ production, and CAR-T cell proliferation.

High avidity interaction with target cells drives CAR-T proliferation and thereby sustained effector function

To compare activation profiles, we first measured CAR-T cytokine secretion in response to antigen-bright LAN-1 and Kelly neuroblastoma cell lines. Unexpectedly, despite having seen high and equivalent killing of the targets by all three CARs in short-term killing assays (Fig. 3b), the lower avidity MGA271 produced significantly lower levels of IFN-γ and IL-2 than TE9 and 376.96 CAR-T (Fig. 4a, b). MGA271 CAR-T cell numbers declined throughout the assay in a manner that was indistinguishable from NTD T cells, whilst TE9 and 376.96 CAR-T proliferated at each challenge with targets (Fig. 4c). The relatively attenuated MGA271 CAR-T proliferation was also seen when challenging CAR-T cells at low E:T ratios with either LAN-1 or SK-N-SH neuroblastoma (Fig. 4d).

The pattern of CAR-T persistence and proliferation in the 691-T or -B neuroblastoma tumoroid re-challenge assays (Fig. 4e, f) mirrored this differential cytokine response of the different binders. MGA271, but not TE9 and 376.96 CAR-T cell numbers declined steadily over time Supplementary Fig. 7)—even in conditions where the MGA271 CAR-T had initially mediated high-level killing at first challenge, such as was seen against 691-T in Fig. 3d, f.

To evaluate whether B7H3 CAR-T responses to brain tumor targets are similar, we identified three different medulloblastoma models with a range of antigen densities (Fig. 5a). All were B7H3^med or B7H3^med-hi. CAR-T cytotoxicity upon single challenge with these targets was equivalently high across all scFv's at a range of E:T ratios (Supplementary Fig. 8). As was the case with the neuroblastoma targets, however, there were differences in antigen-induced CAR-T proliferation between the binders. Low-avidity MGA271 proliferated significantly less than TE9 or 376.96 CAR-T, at a level that was not significantly greater than that of NTD T cells (Fig. 5b). All CAR-T products that were used in this and other assays were viability quality-

controlled to ensure that T cell viability does not act as a confounding factor. In this instance, CAR-T cells used across the various donors and conditions were 93-96% viable, as measured by automated Countess cell counting slides.
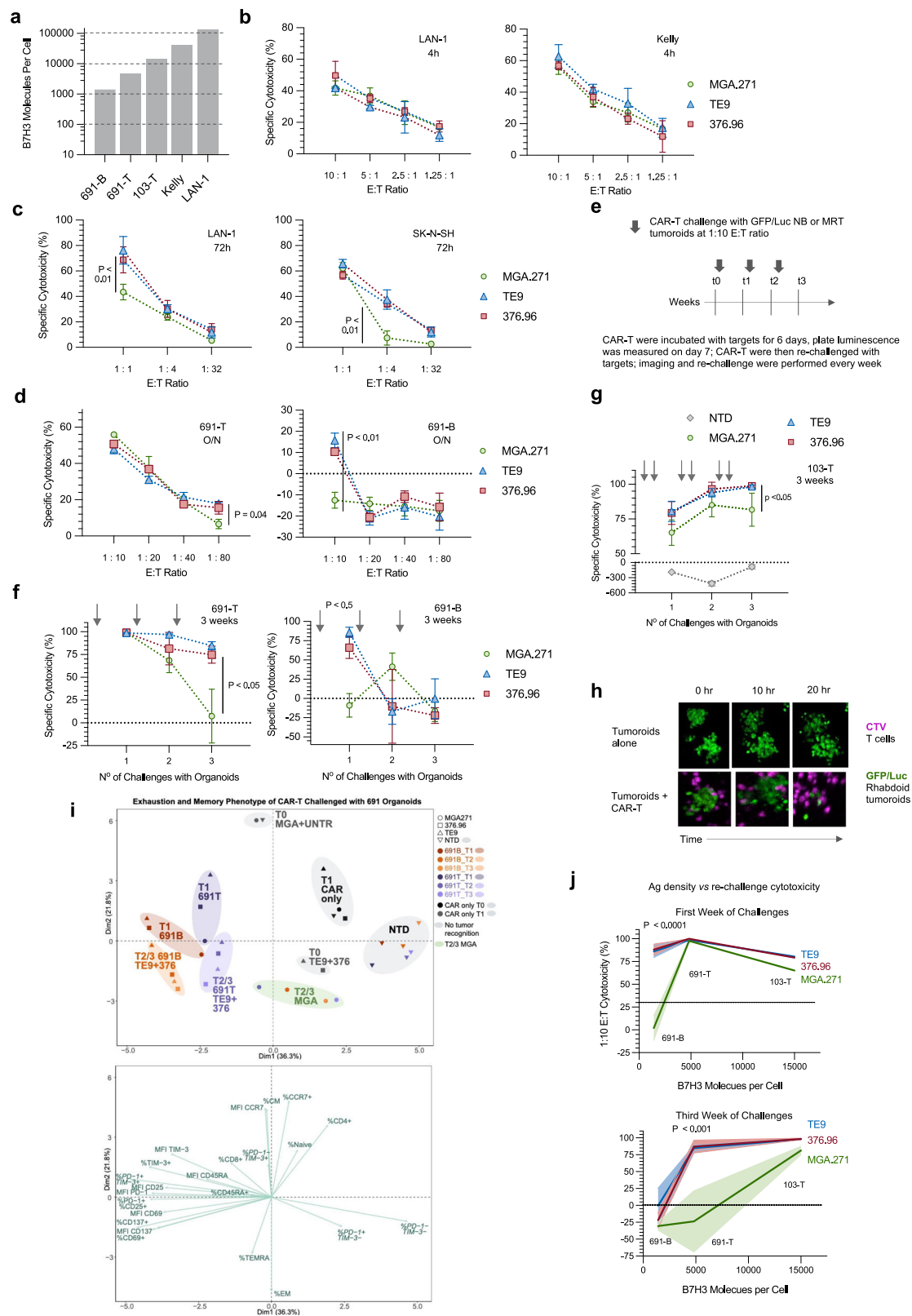
Proliferation for all CAR-T cells was proportionate with antigen expression, and the required B7H3 threshold for driving an increase in T cell numbers was higher for MGA271 than TE9 and 376.96 CAR-T (Fig. 5c). Linking CAR-T proliferation to avidity measurements from Fig. 2 revealed that for both Med8A and LAN-1 targets, which are both relatively antigen bright, avidity appeared predictive of subsequent T cell proliferation (Fig. 5d).

High cellular avidity, determined by scFv affinity, CAR expression, and B7H3 antigen density, drives elimination of antigen-dim targets

To identify the threshold of B7H3 antigen density for binder-dependent CAR-T functionality within the context of the same target cell, we generated a cell line that expresses a range of B7H3 densities by transducing SupT1 cells with 4-Ig B7H3 (Fig. 6a). The SupT1 cells were also transduced with a transgene encoding eGFP and luciferase to enable cytotoxicity evaluation by luminescence. Resulting SupT1-B7H3^range contained cells with a range of B7H3 antigen densities from negative to ultra-high (Fig. 6b). CAR-T were challenged with SupT1-B7H3^range cells at a 1:1 E:T ratio daily for a week to mimic continued exposure to tumor (Fig. 6c).

While all CAR-T cells exhibited some cytotoxicity against SupT1-B7H3^range cells, MGA271 killing of targets was consistently lower than that of TE9 and 376.96 CAR-T (Fig. 6d). Of note, in contrast to previous targets assayed, MGA271 CAR-T kept up sustained, if low-level, killing even following seven challenges with targets. None of the CAR-T killed control SupT1-WT cells (Supplementary Fig. 9a). Substantial 376.96 and TE9 proliferation was seen as target challenge progressed, whilst more modest MGA271 proliferation was observed (Fig. 6e). The antigen dependency of the proliferation was demonstrated by the lack of response in the presence of SupT1-WT targets (Supplementary Fig. 9b) or unstimulated conditions (Fig. 6f). TE9 and 376.96 CAR-T produced significantly more IL-2 and IFN-γ than MGA271 after the initial challenge with SupT1-B7H3^range targets (Fig. 6g).

CAR-T/tumor cocultures were harvested after the fifth challenge, and residual SupT1-B7H3^range expression of B7H3 was measured. Figure 6h shows concatenated B7H3 expression on GFP-positive SupT1 cells across the CAR groups. While TE9 and 376.96 CAR-T cultures contained few or no residual B7H3-positive targets, MGA271 CAR-exposed SupT1 cells maintained a range of B7H3 expression. Compared to the NTD T cell condition, MGA271 eliminated only the antigen-high SupT1 targets (Fig. 6h, i). We observed the same

differences when performing a 72 h in vitro co-culture with SupT1-B7H3^{range} cells at a lower E:T ratio of 1:4 (Supplementary Fig. 9c–e).

In an intravenous model of SupT1-B7H3^{range} leukemia/lymphoma (Fig. 6j), both SupT1-B7H3^{-range} and CAR-T cells were present at only low levels in blood at day 9 post engraftment (Supplemental Fig. 10b). At day 14, SupT1^{-range} cells in bone marrow showed significantly higher levels of B7H3 in MGA271 CAR-T treated mice than for 376.96 or TE9

CAR-T (Fig. 6k, l and Supplementary Fig. 10a) suggesting in vivo tumor editing by MGA271 CAR-T to leave antigen-dim tumor, whilst the 376-96 and TE9 CAR-T cells left only antigen-negative tumor. Consistent with the TE9 and 376.96 CAR-T cells having eradicated all antigen-positive cells, those CAR-T were virtually undetectable in post treatment bone marrow whilst MGA271 were still detectable, albeit at low levels, suggesting ongoing but ineffective interaction with antigen (Fig.

Fig. 3 | TE9 and 376.96, but not MGA271 CAR-T, respond to B7H3 ultra-dim tumor targets in serial re-challenge cytotoxicity assays. a Number of B7H3 molecules/cell (QuantiBright flow cytometry assay) for evaluated target cell lines n = at least 3 technical replicates per cell line. **b** CAR-T cell cytotoxicity against LAN-1 and Kelly neuroblastoma cell lines at high E:T ratios (4 h ^{51}Cr release assay). "Specific cytotoxicity" denotes cytotoxicity relative to non-transduced (NTD) T cell controls (mean ± SEM, N = 3 donors, two-way ANOVA). **c** CAR-T cell cytotoxicity against LAN-1 and SK-N-SH neuroblastoma cell lines at low E:T ratios (72 h flow cytometry-based cytotoxicity assay). "Specific cytotoxicity" denotes cytotoxicity relative to non-transduced (NTD) T cell controls (mean ± SEM, N = 3 donors (two technical replicates per donor), Two-way ANOVA for LAN1 376 vs MGA p = 0.003, TE9 vs MGA p = 0.02 for SKNSH 376 vs MGA p = 0.001, TE9 vs MGA p = 0.004). **d** CAR-T cell cytotoxicity against GFP/Luc-engineered tumoroids by overnight luminescence-based assay. "Specific cytotoxicity" denotes cytotoxicity relative to NTD T cell controls (mean ± SEM, n = 2 biological replicates for MGA and 376, n = 1 biological replicate for TE9: representative of two independent experiments, each with an n = 3 technical replicates; two-way ANOVA 376 vs MGA p = 0.0017, TE9 vs MGA p = 0.0002). **e–g** Re-challenge assay timecourse (**e**), against **f** neuroblastoma tumoroids and **g** malignant rhabdoid tumoroids (MRT); gray arrows indicate re-challenge with tumor. In (**f**), data were mean ± SEM of n = 2 biological replicates for MGA and 376, n = 1 biological replicate for TE9: two independent experiments, each with an n = 3 technical replicates; "specific cytotoxicity" denotes cytotoxicity relative to NTD T cell controls; two-way ANOVA; uncorrected Fisher's LSD with a single

pooled variance in (**f**) 376 vs MGA p = 0.002, TE9 vs MGA p = 0.0055. In **g**, "specific cytotoxicity" denotes cytotoxicity relative to tumor alone controls plated in parallel, data were mean ± SEM, N = 1 independent T cell donor across three experimental replicates: two-way ANOVA; Dunnett's multiple comparisons test, with a single pooled variance 376 vs MGA p = 0.016, TE9 vs MGA p = 0.02.
h Representative microscopy images of 103-T Malignant Rhabdoid Tumor tumoroid killing by TE9 CAR-T. The experiment was conducted once at this E:T ratio.
i Flow cytometric analysis after CAR-T cell co-culture (691-B and 691-T tumoroids shown in (**f**)) was pooled across the replicates, dimensionality reduced using PCA, and grouped according to CAR, target and time-point (T0, pre-challenge with targets; T1, 1 week of challenge; T2, 2 weeks of challenge; T3, 3 weeks of challenge). The colored dots represent concatenated individual conditions, whereas the text in green is descriptive of the phenotype each PCA quadrant is enriched for. The arrows indicate the strength (arrow length) and direction of the contribution of each phenotypical marker to the two principal components, indicating that samples on the same side as a certain arrow have a high expression of that phenotypic marker; n = 1 biological replicate from a single experimental run, of three pooled technical replicates. **j** 1:10 E:T ratio cytotoxicity for the first and 3rd week challenge from the assays showed in panels (**f, g**) plotted against antigen density (Quantibright); line = mean cytotoxicity, shaded area = SEM:n = 2 biological replicates for MGA and 376, n = 1 biological replicate for TE9: two independent experiments, each with an n = 3 technical replicates.

6m). Due to outgrowth of SupT1-B7H3-negative cells in all CAR conditions, all mice had detectable tumor burden at time of endpoint (Supplemental Fig. 10c).

We then aimed to determine the relationship between T effector function (cytokine secretion and proliferation) and CAR avidity in the SupT1-B7H3^{-range} model. CAR-T fold-proliferation over five challenges with targets correlated with IL-2 production at the time of the initial target challenge, though 376.96 CARs were more consistent initial IL-2 producers than TE9 CARs (Fig. 6n). The avidity of CAR-T interaction with SupT1-B7H3^{hi} targets shown in Fig. 2 correlated with both IL-2 production and proliferation in response to SupT1-B7H3^{range} cells (Fig. 6o, p). A similarly strong but inverse correlation was observed between avidity of interaction and the antigen expression on residual SupT1-B7H3^{range} cells following serial re-challenge (Fig. 6q). Taken together, the data indicate that for each cell target engaged by a standard CD28ζ CAR-T cell, there is a threshold of avidity required for sufficient cytokine and proliferation response to allow for expansion and effective cytotoxicity on target re-challenge. We next examined the impact of scFv on B7H3 CAR-T functionality at the single-cell level.

High "on-rate" is associated with high CD8$^{±}$ CAR-T/tumoroid contact duration and rapid cytotoxicity against B7H3^{dim} targets
BEHAV3D, a multispectral, 3D image-based platform, is designed to live-track the efficacy and mode of action of cellular immunotherapy at the single-cell level. BEHAV3D was used to track anti-B7H3 CAR-T functionality over three challenges with 691-B and 691-T tumor targets. Cultures were imaged during the first (day 0) and third (day 7) challenge with targets, and the series of images was then processed for CAR-T behavior using a bioinformatic pipeline, developed by Anne Rios and colleagues[31] (the assay setup is illustrated in Fig. 7a, b and Supplementary Fig. 11). CAR-T cell behavior was tracked across six different parameters, shown in Fig. 7b. Video compilations of day 0 and day 7 CAR-T/tumoroid cocultures can be viewed in Supplementary Videos 1–24.

CAR-T/tumoroid interactions leading to tumoroid death were evident for all conditions (representative cocultures images shown in Fig. 7c). In analysis of behaviors against B7H3^{dim} 691-B tumoroids, striking and unexpected differences were seen between the binders, and between CD4^{+} and CD8^{+} T cells. Plotting the cumulative CD8^{+} CAR-T/tumoroid contact since initiation of the day 0 co-culture showed that TE9 and 376.96 CD8^{+} CAR-T spent significantly longer in contact with B7H3^{dim} 691-B tumoroids than MGA271 CD8^{+} CAR-T did (Fig. 7d). A

summation of total CD8^{+} CAR-T/691-B contact time during the entire day-0 analysis confirmed this difference between binders (Fig. 7f). This cumulative contact score correlated with the cytotoxicity of respective binder-CAR-T constructs against these B7H3^{dim} 691-B targets in an overnight 1:10 E:T killing assay (Fig. 7d, e). In contrast, all CD8^{+} CAR-T showed similar contact time and cytotoxicity against higher antigen density 691-T tumoroids (Fig. 7d–f). Analyzing cytotoxicity by detection of organoid death during the imaging (tumor cell conversion from "yellow" to "red" in Fig. 7c) confirmed the observation that TE9 CAR-T were the most rapid at killing B7H3^{dim} 691-B tumoroids, followed by 376.96 and MGA271 CAR-T cells. In contrast, all CAR-T cells were equally rapid at killing 691-T tumoroids of higher antigen density (Fig. 7g).

There were no differences between binders in terms of the number of new CAR-T contacts during the 800-min data collection, using either tumoroid model (Supplementary Fig. 12a). Hence, the finding of the highest total T cell/tumoroid contact time of the TE9 CD8 CAR-T cells (Fig. 7f) implied TE9 was the binder conferring the longest duration of individual contacts. Consistent with this observation, TE9 CD8^{+} CAR-T cells also showed the lowest displacement distance (Fig. 7h) and speed of displacement (Fig. 7i). whilst MGA271 had the shortest and 376.96 were intermediate (Fig. 7f–i). This ranking of tumor interaction duration of TE9 > 376.96 > MGA271 when targeting low antigen density targets correlated with the cytotoxicity, avidity, and binder association rate constant (Supplementary Fig. 12b). These data suggest that high avidity anti-B7H3 binder CD8^{+} CAR-T cells stay longer in contact with low antigen tumoroids to facilitate more efficient killing.

Compared to CD8^{+} CAR-T cells, CD4^{+} CAR-T cells showed greater displacement and reduced tumoroid contact, and this was observed in both models of higher and lower antigen density, respectively (Fig. 7f, h, i). Moreover, in CD4^{+} CAR-T, the influence of the respective binders on tumoroid contact and displacement was variable, consistent with CD4^{+} CAR-T cells having a lesser role in tumoroid contact and direct cytotoxicity, as described previously using BEHAV3D analysis[25] (Fig. 7f, h, i). While more mobile overall, CD4^{+} CAR-T cells did not engage in CAR-T/CAR-T interaction more than CD8^{+} CAR-T cells (Supplementary Fig. 12c).

Distinct CAR-T cell characteristics revealed by dimensionality reduction of behavioral parameters
To extract behavioral patterns and dynamics, the day 0 BEHAV3D tumor challenge imaging data was clustered using UMAP (Supplementary Fig. 13a), revealing six CAR-T behavior types: "tumoroid
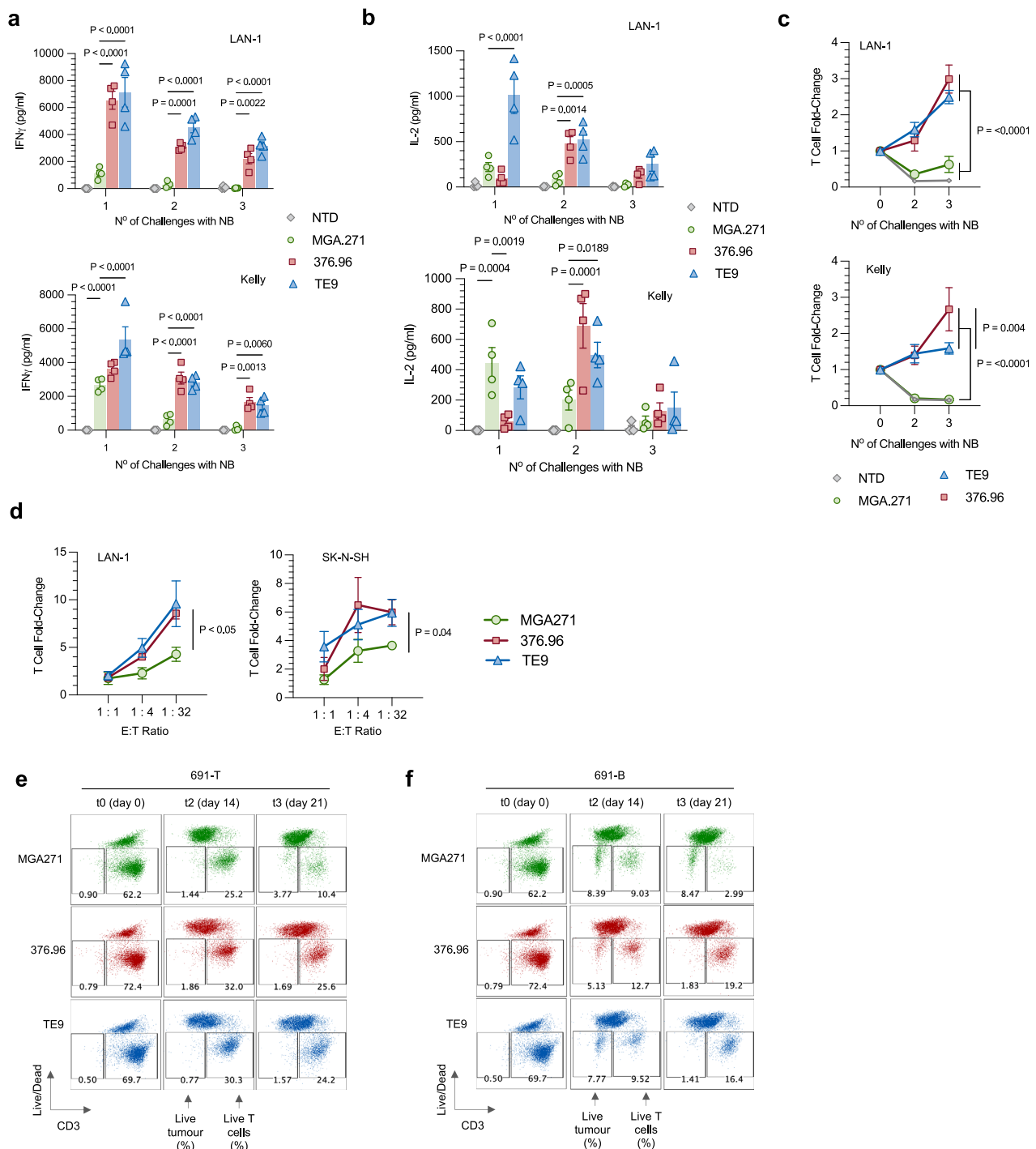
Fig. 4 | High avidity interaction with target cells drives CAR-T proliferation and sustained effector function. a, **b** CAR-T cells stimulated with irradiated LAN-1 or Kelly neuroblastoma cells at a 1:1 E:T ratio every 7 days; IFN-γ (**a**) and IL-2 (**b**) measured in 24 h post stimulation supernatants (mean ± SEM, N = 3 independent donors, two-way ANOVA. **c** T cell numbers in same cocultures evaluated using precision count beads and flow cytometry (mean ± SEM, N = 3 independent donors, two-way ANOVA. **d** T cell counts were performed using the same precision count bead methodology in 72 h low E:T ratio LAN-1 and SK-N-SH cocultures, cytotoxicity

for which is shown in Fig. 3c (mean ± SEM, N = 3 independent donors, two-way ANOVA: for LAN1 376 vs MGA 0.0168, TE9 vs MGA p = 0.0036). **e**, **f** Relative T cell proportions measured using flow cytometry in 691-B and 691-T tumor cocultures over 3 weeks of weekly tumor challenges at an E:T ratio of 1:10. Gated on single cells of harvested cultures (T cells and tumor cells) at days 14 and 21 and gated on all cells at day 0 prior to targets being added, representative dot plots from one donor CAR-T are shown. The numbers shown on the plots are indicative of % live tumor and % live T cells within each culture of total cells.

engagers" (cluster 1), "multi-taskers" (clusters 2, 3), "CAR-T engagers" (clusters 4,5), and "dying T cells" (cluster 6) (Fig. 7j). Fitting with the individual cell analysis, the "tumoroid engager" cluster 1 was relatively enriched in CD8$^+$ cells compared to CD4$^+$ and with higher antigen density 691-T compared with 691-B targets (Fig. 7k). Moreover, TE9

and 376.96 binder CD8$^+$ T cells consistently exhibited more cluster 1-type tumor engager behavior than MGA271 CAR-T against both tumor targets, and further exhibited more "multi-tasker" behavior in the 691-B tumoroid co-culture. These differences between binders were less apparent in the CD4$^+$ CAR-T context.
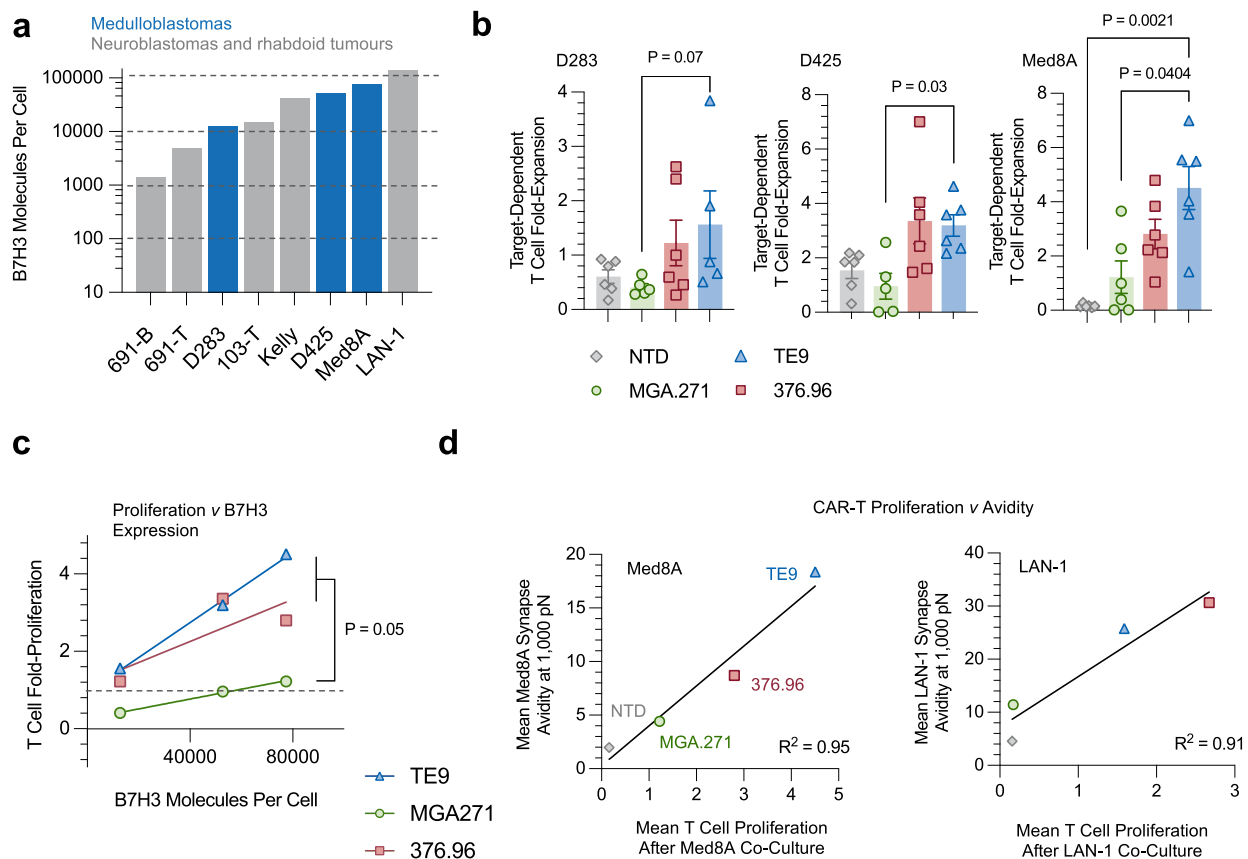
Fig. 5 | High avidity interactions drive CAR-T proliferation and cytotoxicity in brain tumor models. a B7H3 molecules per cell were quantified using QuantiBright flow cytometry assay; brain tumor targets in blue, neuroblastoma and rhabdoid tumor targets in gray. **b** T cell proliferation in response to live brain tumor cell challenge at a 1:1 E:T ratio quantified after 6 days of co-culture (mean ± SEM, three independent T cell donors across two experimental replicates, Kruskal–Wallis test). **c** T cell fold-expansion plotted against number of B7H3 molecules per target cell; symbols represent mean proliferation of the different donors and replicates; lines are simple linear regression curves. **d** Mean fold-proliferation of CAR-T cells against Med8a and LAN-1 cells plotted against mean avidity at 1000 pN for the two cell lines. Symbols represent the mean proliferation of the different donors and replicates; the lines are simple linear regression curves.
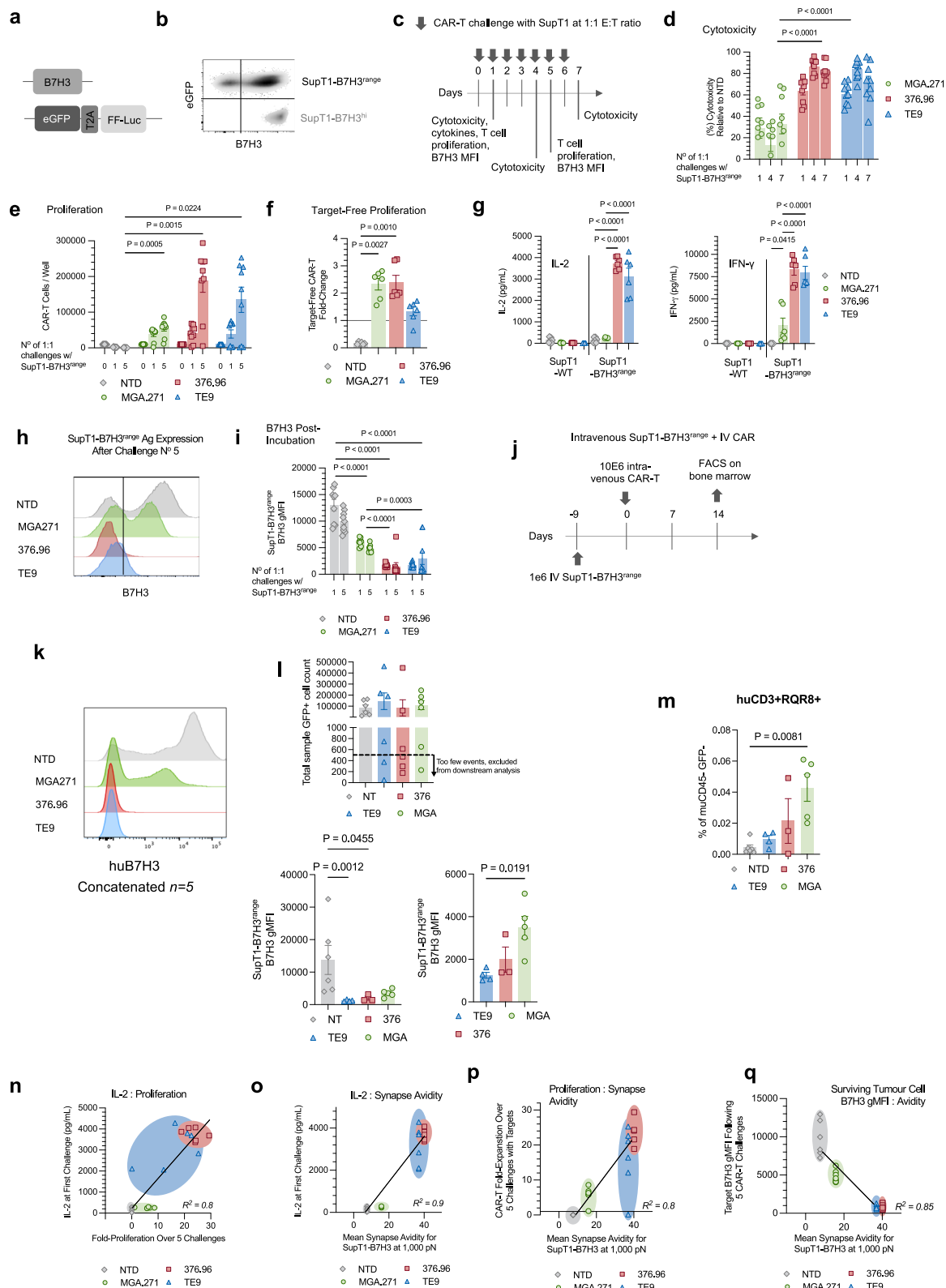
CAR-T behavior was then compared between the two analyzed timepoints (day 0 and day 7). Day 7 CAR-T behavior was reduced using UMAP into 7 clusters across the two imaging sessions (Supplementary Fig. 13b), which grouped into "organoid interaction" (clusters A, B, C, D), "CAR-T interaction" (clusters E, F), and cell death (cluster G) (Supplementary Fig. 13c). Strikingly, no consistent differences between the CAR-T binders or even CD4+ vs CD8+ T cells remained evident at day 7 (Supplementary Fig. 13d). This narrowing of CAR-T phenotype was evident when comparing the trajectory of tumoroid death over the day 0 and day 7 imaging sessions, pooling data from all three binders and target types (Fig. 7l). A broad range of tumor killing trajectory was seen at day 0 whilst at day 7 all CARs mediated rapid tumor clearance. This apparent ability of low avidity MGA271 CAR-T to control low antigen density tumor at day 7 is most likely due to artificially resetting the effector to target ratio at each tumor challenge with re-sorted viable CAR-T cells.

The dimensionality reduction BEHAV3D analysis reflects the broad conclusion that high avidity of CD8+ T CAR-T cells equips them for longer interactions with low antigen density targets, which facilitates sustained cytotoxic activity. The data support our hypothesis that the differences in CAR-T functionality seen in vivo and in vitro assays are caused not by variation in binder-driven functional exhaustion, but rather by the differential ability of the CAR-T constructs to proliferate and engage in serial tumor cytotoxicity.

Discussion

The capacity of CAR-T cells to engage in efficient serial killing through repeated successful interactions with tumor cells without inducing T cell exhaustion may be the defining feature of a successful solid cancer CAR-T construct. The CAR-T to tumor interaction encompasses a CAR immune synapse, wherein the initial contact between T cell and tumor is stabilized by the CAR antibody to target antigen binding interaction, which develops into a cluster of engaged CAR constructs. It is likely that the strength of this interaction, as well as the number of target antigens, will determine whether the synapse becomes functional; i.e., triggers death of the target cell through release of cytolytic granules concomitant with T cell signaling to promote proliferation and cytokine secretion[32,33].

Successful formation of a synapse leads to the exclusion of phosphatases (e.g., CD45) and the recruitment of src family kinases (e.g., lck), resulting in phosphorylation of CD3ζ chain ITAMs within the CAR molecule, and subsequent signaling. An efficient and high-quality CAR-T immune synapse might be one that is strong enough to induce death of the target and short-lived enough to induce a "goldilocks" quantity and quality of T cell signaling that promotes activation without exhaustion. Immune synapse quality is likely affected by the nature of the initiating antibody-to-antigen interaction. Recent progress in CAR-T/target interaction tracking at the single cell level, on platforms such as BEHAV3D[31], has enabled a nascent understanding of the kinetics of immune synapse formation and how synaptic formation

dynamics differ between CD4 and CD8 cells. The relationships between the synapse, the binding properties of the CAR scFv's and the effect of synaptic signaling on T cell activation and exhaustion remain poorly understood.

Cellular avidity is the strength of interaction between a CAR-T cell and its tumor target, which we have measured as the force required to disrupt the interaction. We hypothesized that avidity would be influenced by three factors: the CAR surface expression on CAR-T cells, the target antigen density on the tumor cells, and the affinity of the antibody to the antigen interaction at the single molecular interaction scale. We reasoned that this interplay of factors would be such that none of the parameters alone would be predictive of CAR-T response, but the interaction of the three factors to define functional avidity would be the closest predictor of subsequent T cell function. We

Fig. 6 | High avidity drives the elimination of antigen-dim targets. a Constructs for generation of B7H3 and GFP/luciferase sublines of SupT1 cells. **b** Expression of B7H3 in the unsorted "SupT1-B7H3^{range}" and flow-sorted "SupT1-B7H3^{hi}" cells. **c** Rechallenge assay experimental schematic. **d** Cytotoxicity was measured by luciferase signal as relative to tumor luminescence in the presence of donor-matched non-transduced (NTD) T cells (mean ± SEM, two-way ANOVA). **e** T cell numbers in the same assay following either a range of challenges with tumor targets or **f** target-free (mean ± SEM, two-way ANOVA). **g** Cytokine measurements in co-culture supernatants following a single challenge with SupT1-B7H3^{range} targets at a 1:1 E:T ratio (mean ± SEM, two-way ANOVA). **h** B7H3 expression on targets measured using flow cytometry following the fifth re-challenge. Shown are concatenated histograms that were generated by combining flow data adjusted for 10,000 SupT1 cells per sample. **i** The same SupT1-B7H3^{range} positivity for antigen as analyzed in each sample separately (mean represents geometric mean fluorescence intensity (gMFI) ± SEM, two-way ANOVA). **j** Schematic of leukemia model using SupT1-B7H3^{range} T cell lymphoma cells. **k, l** Concatenated histograms (**k**) and graphical representation (**l**) showing B7H3 expression in gated SupT1 tumor cells in bone marrow at day 14 following CAR-T cell infusion. The samples with 500 or fewer gated tumor cell events were uniformly excluded from quantitation, as shown: error bars show SEM: two-way ANOVA. **m** Quantification of CAR-T cells in bone marrow at day 14 post-T cells; $N = 5$, error bars show SEM, two-way ANOVA. **n** Respective CAR fold-proliferation in response to five challenges with SupT1-B7H3^{range} targets plotted against IL-2 production following the initial challenge. **o** IL-2 production after first challenge plotted against the mean avidity for SupT1-B7H3^{hi} targets at 1000 pN. **p** Proliferation after five challenges with targets was plotted against the mean avidity that the respective CARs achieved when combined with SupT1-B7H3^{hi} targets at 1000 pN. **q** SupT1-B7H3^{range} cell B7H3 gMFI after five challenges with targets was plotted against the mean avidity that the respective CARs achieved when combined with SupT1-B7H3^{hi} targets at 1000 pN. In **n–q** each symbol represents an individual donor experimental replicate, the lines are simple linear regressions. For all data in the panels: $N = 4$ independent donors across four experimental replicates.

evaluated the relationship of antibody to antigen binding properties, as both affinity (Biacore surface plasmon resonance) and cellular avidity (Lumicks) measurements against a range of antigen densities. Two binders of similar affinity (K_D) had quite differing rate constants of association and dissociation with similar avidity (TE9 and 376.96), whilst a third of modestly lower affinity also demonstrated low avidity (MGA271). Several previous studies have investigated the avidity of CAR-T cells using the Lumicks platform[16,34]. For example, the group of Maher et al. studied a range of anti-CD19 binders in the context of leukemia therapy using conventional second-generation CARs co-expressing a 4-1BB chimeric co-stimulatory receptor[34]. Interestingly, intermediate avidity CAR-T were identified to have the greatest in vivo capacity to control tumor growth.

Using repeat stimulation assays against suspension cells, monolayers and three-dimensional tumoroid models to recapitulate the repeat antigenic engagement of the tumor environment, we show that low avidity interaction on first tumor encounter results in a weak cytokine and proliferative response. Weak initial response translates into the ultimate failure of expansion and tumor control in stress conditions. In contrast, higher avidity initial interaction in the low antigen density setting results in effective proliferation and serial killing. In the setting of higher antigen density, all CAR-T constructs have a sufficiently high avidity initial interaction to induce expansion and serial killing, although low avidity MGA271 still ultimately has reduced functionality at the end of serial challenges. Previous studies have identified fast off-rate as linked to more efficient and effective CAR-T control[6,19–21] and it is therefore an interesting contrast in our tumoroid studies to note that the quickest construct for tumor control of low antigen density had the longest organoid contact time as well as the fastest on- and off-rates. This apparent discordance might be explained by the multiple cell contacts that single CD8$^+$ CAR-T generate with the multi-cellular tumoroid structures, as previously described using BEHAV3D analysis[31]. Here, a more complex and dynamic interaction of an individual CD8$^+$ CAR-T cell with multiple tumor cell targets within a 3D structure might explain a more complex relationship between avidity and success in tumor control. Future studies in monolayers of adherent cells, although technically more challenging, could provide additional data on the relation between avidity and functionality in real-world cancer settings where CAR-T cells are likely to interact with cells in a full range of three-dimensional arrangements.
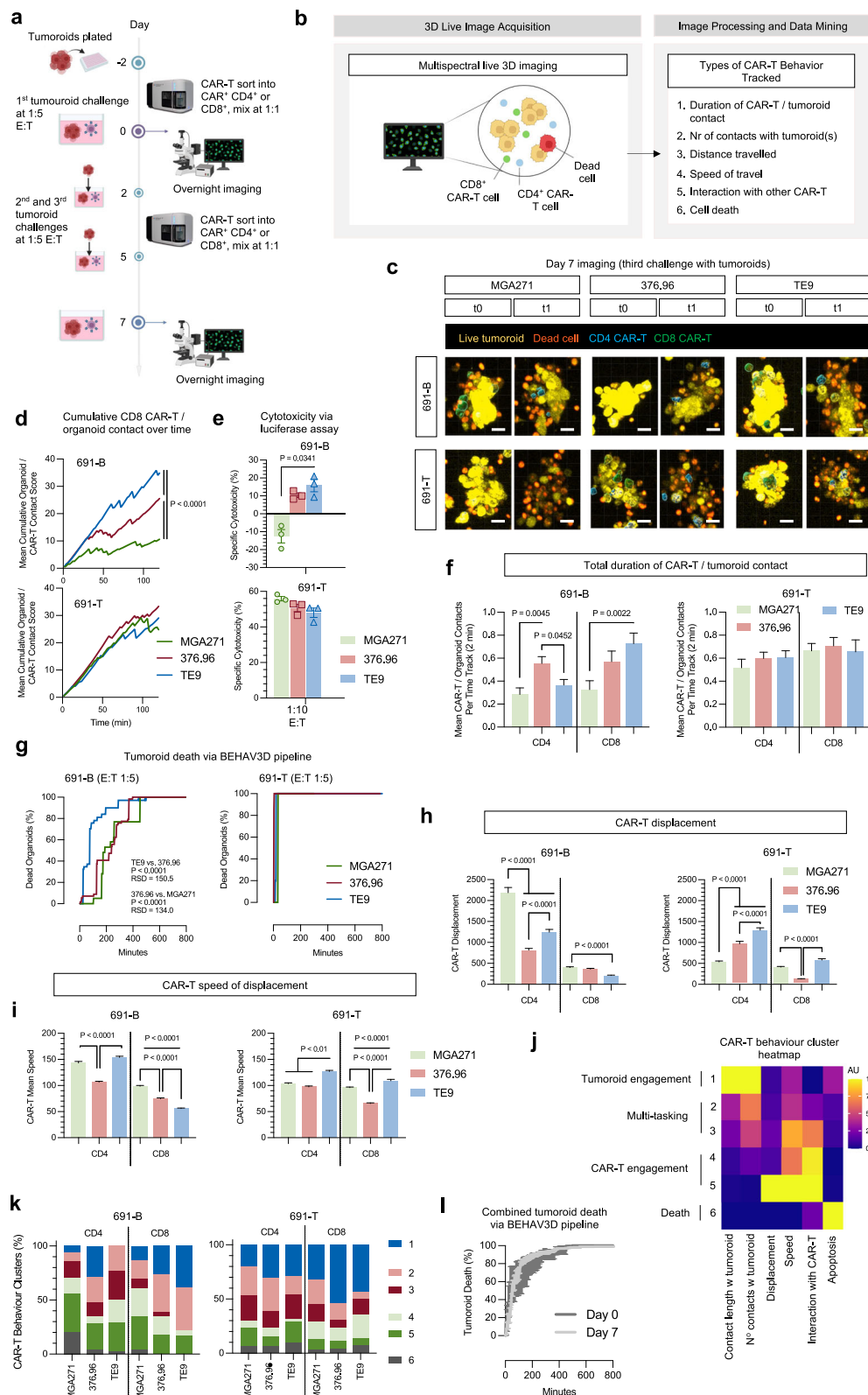
Of note, in the current models, which extend to seven repeat tumor challenges, we have not seen evidence of differences in T cell exhaustion between the three binders. This may be because the repeated antigenic challenges were not sustained long enough, and it is also tempting to speculate that a higher affinity antibody/higher avidity CAR-T cell might have induced exhaustion in the same repeat stimulation experiments. All binders evaluated showed only modest increases in TIM-3$^+$PD-1$^+$ double-positive cells and little evidence of exhaustion induced by signaling in the absence of antigen (tonic signaling). It will be important in future studies to evaluate whether very high avidity binders and/or tonic signaling binders show relative failure associated with increased exhaustion marker expression.

One notable observation was that the TE9 binder, which had similar affinity and avidity to the 376.96 binder, had both the highest on-rate and fastest off-rate. To determine if this impacted the CAR-T/tumor interaction time, we performed BEHAV3D video microscopy analysis. Interestingly, we found that at higher antigen densities, there were no difference in dwell time between the binders. In contrast, at low antigen density, the CD8$^+$ 376.96 and TE9 CAR-T cells had longer dwell times than MGA271 CAR-T, which was consistent with both their greater cytotoxicity and the higher displacement score of the MGA271 CAR-T. The fast on- and off-rates (in single molecule Biacore affinity studies) of TE9 appears to translate into longer tumoroid contact, and leads us to speculate that avidity measurements may prove to be of greater predictive value for CAR-T synapse formation characteristics. A further surprising result was the short tumor dwell time of TE9 CD4$^+$ cells, which appeared to be of less importance in direct cytotoxicity. Overall, these data add to the growing literature wherein, in other model systems or CAR structures, lower avidity has been associated with shorter dwell time and heightened functionality, for example targeting CD19[6]. Further studies are required to confirm these observations with other binders and targets, including detailed evaluation of the role of antigen density in setting activation thresholds, as well as mechanistic studies to determine the significance of differences in avidity between CD4$^+$ and CD8$^+$ CAR-T cells.

B7H3 is an emerging attractive target for cancer immunotherapy due to its bright expression on the surface of a high proportion of cancer cells, its association with poor prognosis, its potential function as an immune regulator, and its relative absence on healthy tissues[35,36]. Interestingly, its cancer specificity seems to extend beyond cancer cells in the tumor environment since several lines of evidence point to its expression in a variety of tumor-infiltrating cells, such as vascular endothelial cells[37]. Hence, the clinical application may extend beyond cancers in which B7H3 has a role as a driver oncogene. All three of the binders evaluated in this study are of clinical relevance and are being evaluated in a range of clinical trials.

There are three important implications of these avidity findings for the clinical activity of these respective binders. The first is the threshold of antigen density for activation. B7H3 is expressed at a low level in some healthy tissues. A lower avidity binder might have an optimal activation threshold to distinguish healthy from tumor tissue to avoid on-target off-tumor toxicity. Secondly, the avidity threshold for activation will be affected by the respective signaling characteristics of the CAR. Further work is needed to dissect this, which could be achieved, for example, by comparing the CAR-T construct with

identical avidity but altered signal strength, through, for example, altering the number of ITAMs. Of note, none of the constructs used in the study shows much evidence of tonic signaling, which could mitigate the poor response to low antigen density through enhancing proliferation. Moreover, work using the MGA271 binder has shown that substitution of the CD8 hinge and transmembrane regions (H/TM) as evaluated in this paper, for CD28 H/TM, within the context of

41BB-CD3ζ signaling, results in significantly improved function against low antigen density targets[7]. Our studies have identified that, in the specific context of SFG gammaretroviral expression and the CD8H/TM-28Z second-generation format, MGA271 is less well expressed on the cell surface, contributing to low avidity. It follows that it is possible that the avidity and function of MGA271 could be significantly higher using different vectors or endodomains due to

Fig. 7 | Higher CAR binder B7H3 avidity is associated with increased CD8$^+$ CAR-T / tumoroid contact duration and more rapid cytotoxicity against B7H3$^{ultra-dim}$ tumoroids. a, b experimental overview· images created with BioRender. (Barisa, M. (2025) https://BioRender.com/ub1tswj). **c** Illustrative stills of tumoroid and T cell clusters at the start (day 0 = t0), and end (day 7 = t1) 800 min imaging sessions. **d** CD8$^+$ CAR-T cell cumulative contact time with 691-B and 691-T organoids was tracked for the first 2 h of the first tumor challenge on day 0. The line represents the mean cumulative tumoroid contact score of all the individual CAR-T cells that were successfully tracked for the full 120 min period (the number of cells tracked in each of the conditions was a mean 31.33 ± 10.8; curves were compared using simple linear regressions). **e** CAR-T cells were incubated with tumoroids overnight at a 1:10 E:T ratio. "Specific cytotoxicity" denotes tumor luminescence relative to matched non-transduced T cell (NTD) controls (mean ± SEM, $N = 3$ independent experimental replicates, Kruskal–Wallis test). **f–i** Respective parameters were tracked for the entire duration (800 min) of the first tumor challenge at day 0. **f** CD4$^+$ and CD8$^+$ CAR-T cell cumulative contact time with 691-B and 691-T organoids (mean ± SEM, $N = 31.5 ± 10.6$ cells per T cell condition, Two-Way ANOVA). **g** Cumulative tumoroid death (conversion from viability dye yellow to red) (a total of 398 incremental timepoints were recorded to track tumoroid apoptosis over the assay; curve comparison was carried out using a Friedman test for P value and rank sum differences (RSD)). **h** CD4$^+$ and CD8$^+$ CAR-T displacement (mean ± SEM, $N = 31.5 ± 10.6$ cells per T cell condition, two-way ANOVA). **i** Mean speed of CD4$^+$ and CD8$^+$ CAR-T displacement (mean ± SEM, $N = 31.5 ± 10.6$ cells per T cell condition, two-way ANOVA). **j** Trends in CAR-T behavior reduced into six clusters using UMAP analysis of behaviors across all the conditions observed in the initial tumor challenge at day 0 and represented as a heatmap. **k** The CAR-T behaviors are broken down by T cell, binder and target type. **l** Pooled data from all CAR constructs against both targets, comparing day 0 and day 7 challenge rate of organoid death.

better cell surface expression. In the current clinical trial NCT05474378 (Mackall and colleagues), the configuration is with CD8 hinge/transmembrane with 41BB costimulation. A second recruiting clinical study (SJ-19-0014; St Jude's, USA; DeRenzo et al.) using MGA271 with CD28ζ is deploying an additional 41BBL costimulation in-trans module[28], whilst trial NCT04185038[15] (Seattle, USA; Vitanza and team) makes use of MGA271 with CD28 H/TM in a second gen 41BB-CD3ζ configuration. Hence, none of the current MGA271 trials are using the configuration in the current paper. Thirdly, higher expression of CAR through the use of higher MOI of virus could increase the avidity of a given binder against targets. Artificially, we ensured equivalent expression levels to allow fair comparison of avidity effects in relation to target antigen density. Higher expression of CAR might increase avidity and functionality. What seems clear is that all CARs require fine-tuning of binders to identify optimal activation thresholds. Avidity measurements may prove an additional valuable parameter for screening constructs for optimal signaling and activation.

Methods
The research in this publication complies with relevant ethical regulations: UK research ethics approval IRAS154668.

Cells lines and culture conditions
All cell lines were cultured in humidified 37 °C in 5% CO$_2$ conditions. Cell lines were thawed and passaged for at least two weeks prior to use in functional assays. Culture mycoplasma tests were performed monthly using the MycoAlert Detection Kit from Lonza. The following Table 1 summarizes the characteristics and culture conditions of the cell lines that were used over the course of this study.

CAR sequences
All CARs were expressed using an SFG backbone in a second-generation RD114 γ-retroviral system. All plasmids were sequenced to verify the absence of unexpected sequence mutations prior to the manufacture of the virus. A diagram of construct structure is shown in Fig. 1a, with all anti-B7H3 CARs expressed in the following format: RQR8-T2A-scFv-CD8αLinker-CD8αTM-CD28endodomain-CD3ζchain. The sequences for the scFv's were obtained from public sources and are summarized in Table 2. To insert these into the CAR backbone, the scFv sequences were ordered as geneblocks and then cloned into a CD8α-CD28-CD3ζ format.

CAR-T cell manufacture
Leukapheresis cones were acquired from NHS Blood and Transplant. PBMCs were separated through Ficoll centrifugation using Lymphoprep (STEMCELL Technologies). PBMCs were washed, and residual red cells were lysed with ACK Lysis buffer (Thermo Fisher Scientific). NK cells were depleted using magnetic CD56 depletion beads (Miltenyi Biotec) and LD depletion columns (Miltenyi Biotec).

PBMCs were suspended in RPMI1640 containing 10% FCS and 1x L-glutamine at a concentration of $1 × 10^6$ cells/mL, and then activated with 0.5 mg/mL of anti-CD3 (clone: OKT-3; Miltenyi Biotec) and anti-CD28 antibodies (clone: CD28.2; Miltenyi Biotec). Forty-eight hours before transduction and on the day of transduction, 100 IU/mL recombinant human IL-2 (Proleukin, Novartis) was added. T cells were transduced with the γ-retroviral SFG constructs following plating on retronectin (Takara Bio)-coated plates and spinoculation. Transduction efficiency was measured three days after transduction using flow cytometry by staining for RQR8 (clone: QBNED10; R&D BioSystems). T cell populations were not corrected for transduction efficiency in functional assays. Transduction efficiencies of >50% were routinely achieved. Expanding CAR-T cell IL-2 media was replenished every two days. Expansions were harvested at day 10–12 following culture initiation and cryopreserved in 10% DMSO complete media. When initiating in vitro or in vivo functional assays, CAR-T cells were thawed in pre-warmed IL-2 (100 IU/mL) complete media (RPMI1640, 10% FCS), rested overnight and then counted. CAR-T E:T ratios were based on the number of viable T cells after overnight rest. Cryopreserved CAR-T recovery after overnight rest (relative to the number of CAR-T that were frozen down) was routinely 50–60%, with a ~90% viability. Cell counting was determined by a Countess 3 automated cell counter (Invitrogen), where cells were diluted in 0.4% Trypan Blue (Invitrogen) and viability was measured through its machine-learning image analysis algorithm.

Animal studies
Animal protocols were approved by local institutional research committees and were in accordance with UK Home Office guidelines. Animals were housed in a temperature and humidity-controlled environment within IVC cages. A maximum tumor diameter of 15 mm was not exceeded. Mixed male and female NSG mice aged between 6 and 8 weeks were supplied by Charles River. All experiments were carried out under UK home office licenses project license number 15981/01, and personal license numbers I13398879, P2E645DD9, I83870811, I27052867, I8C20AD0D, and I754094BC. Individual researchers making tumor measurements were blinded to group identity.

For the LAN-1 in vivo study, NSG mice were injected with $1 × 10^6$ LAN-1-BFP/Luc in Matrigel (Corning) subcutaneously into the flank. CAR-T cells ($1 × 10^7$) were injected intravenously into the tail vein at day 10 following tumor engraftment (treatment schedule illustrated in Fig. 1e). Tumor size was monitored twice a week with digital callipers. Mice were given 200 uL luciferin (Thermo Fisher Scientific) into the scruff and imaged using a PhotonIMAGERTM optical imaging system (Biospace Lab) weekly. Animal sacrifice was initiated upon reaching either a tumor diameter of >15 mm in any direction (as measured by callipers) or the appearance of tumor burden toxicity that exceeds our animal welfare standards (>15% weight loss, change in activity, ataxia, dehydration, loss of normal gait, grimacing).

Table 1 | List of cell lines

Cell Line ID	Type of Cancer	Source	RRID	Culture Media
LAN-1 (LA-N-1)	Neuroblastoma	ECACC	CVCL_1827	RPMI1640 (Gibco) + 10% FCS (Gibco)
Med8A (MED-MEB-8A) wild type	Medulloblastoma	Gift from Michael Taylor, The Hospital for Sick Children, Canada	CVCL_M137	DMEM (Gibco) + 10% FCS + 1x Glutamax (Gibco)
Med8A GFP/Luc	Medulloblastoma	Derived from Med8A wild type by RD114 γ-retroviral transduction with GFP/Luc	None	DMEM (Gibco) + 10% FCS + 1x Glutamax (Gibco)
Kelly	Neuroblastoma	Gift from Andrew Stoker, UCL, UK	CVCL_2092	RPMI1640 + 10% FCS
SupT1 wild type	Childhood T lymphoblastic lymphoma	ECACC	CVCL_1714	RPMI1640 + 10% FCS
SupT1-B7H3^hi	Childhood T lymphoblastic lymphoma	Derived from SupT1 wild type by RD114 γ-retroviral transduction with 4-Ig B7H3 (Sinobiological), followed by flow cytometric sorting	None	RPMI1640 + 10% FCS
SupT1-B7H3^ange GFP/Luc	Childhood T lymphoblastic lymphoma	Derived from SupT1 wild type by RD114 γ-retroviral transduction with GFP/Luc followed by flow cytometric sorting, then 4-Ig B7H3 (Sinobiological) without sorting	None	RPMI1640 + 10% FCS
691-T (AMC691-T) wild type	Neuroblastoma	Gift from Jan Molenaar (Utrecht)	None	'Neurosphere medium': DMEM-GlutaMAX supplemented with 20% Ham's F-12 nutrient mixture, 2% B27 supplement minus vitamin A, 1% N-2 Supplement, 100 U/mL penicillin, 100 mg/mL streptomycin, 300 ng/mL insulin-like growth factor (IGF-1), 40 ng/mL fibroblast growth factor-basic (FGF-2), 20 ng/mL epidermal growth factor (EGF), 10 ng/mL platelet-derived growth factor-AA (PDGF-AA) and 10 ng/mL platelet-derived growth factor-BB (PDGF-BB)
691-T (AMC691-T) GFP/Luc	Neuroblastoma	Gift from Jan Molenaar (Utrecht)	None	'Neurosphere medium'
691-B (AMC691-B)	Neuroblastoma	Gift from Jan Molenaar (Utrecht)	None	'Neurosphere medium'
691-B (AMC691-B) GFP/Luc	Neuroblastoma	Gift from Jan Molenaar (Utrecht)	None	'Neurosphere medium'
103-T wild type	Malignant rhabdoid tumor	Gift from Jarno Drost (Utrecht)	None	'MRT medium'[31,32]: MRT tumoroids were cultured in droplets of growth factor-reduced basement membrane extract (BME) Type 2 (R&D Systems) in kidney tumoroid medium (KOM) (Advanced Dulbecco's Modified Eagle Medium (DMEM)/F-12 (Gibco) containing 1X GlutaMAX (Thermo Fisher Scientific), 10 mM HEPES (Thermo Fisher Scientific) and 1X Penicillin-Streptomycin (P/S) (Merck Millipore), supplemented with 10% R-spondin–conditioned medium, 1.5% B27 supplement (Gibco), 50 ng/mL epidermal growth factor (EGF) (PeproTech), 50 ng/mL fibroblast growth factor (FGF-)2 (PeproTech), 1.25 mM N-acetylcysteine (Sigma), 10 M Rho-associated coiled–coil containing protein kinase (ROCK) inhibitor Y-27632 (Abmole) and 5 uM A83-01 (Tocris Bioscience))
103-T Luc	Malignant rhabdoid tumor	Gift from Jarno Drost (Utrecht); derived from 103-T wild type by lentiviral transduction with pLKO.1-UbC-luciferase blast and pLV-H2B-mNeon-puro cassettes[33,34]	None	'MRT medium'
D283 wild type	Medulloblastoma	Gift from Michael Taylor, The Hospital for Sick Children, Canada	CVCL_1155	DMEM (Gibco) + 10% FCS + 1x Glutamax (Gibco)
D283 GFP/Luc	Medulloblastoma	Derived from D283 wild type by RD114 γ-retroviral transduction with GFP/Luc	None	DMEM (Gibco) + 10% FCS + 1x Glutamax (Gibco)
D425 wild type	Medulloblastoma	Gift from Michael Taylor, The Hospital for Sick Children, Canada	CVCL_1275	DMEM (Gibco) + 10% FCS + 1x Glutamax (Gibco)
D425 GFP/Luc	Medulloblastoma	Derived from D425 wild type by RD114 γ-retroviral transduction with GFP/Luc	None	DMEM (Gibco) + 10% FCS + 1x Glutamax (Gibco)
293-T (HEK293T)	Transformed cell line	ATCC	CVCL_0063	IMDM + 10% FCS

Table 2 | CAR scFv sequences

scFv ID	Full CAR Amino Acid Sequence	Source of scFv Sequence
MGA271	EVQLVESGGGLVQPGGSLRLSCAASGFTFSSFGMHWVRQAPGKGLE-WVAYISSDSSAIYYADTVKGRFTISRDNAKNSLYLQMNSLRDEDTAVYYCGR-GRENIYYGSRLDYWGQGTTVTVSSGGGGSGGGGSGGGGSDIQLTQSPSFLSASVGDRVTITCK-ASQNVDTNVAWYQQKPGKAPKALIYSASYR-YSGVPSRFSGSGSGTDFTLTISSLQPEDFATYYCQQYNNYPFTFGQGTKLEI-KAAAADPTTTPAPRPPTPAPTIASQPLSLRPEACRPAAGGAVHTRGLDFACDIYIWA-PLAGTCGVLLLSLVITLYRTRSKRSRLLHSDYMNMTPRRPGPTRKHYQPYAPPRDFAAYRSRVKFSRSADAPAYQQGQNQLY-NELNLGRREEYDVLDKRRGRDPEMGGKPRRKNPQEGLYNELQKDKMAEAYSEIGMKGERRRGKGHDGLYQGLSTATKDTYDALHMQALPPR*	Macrogenics Inc Patent "US9441049B2"[35]; development described by Loo and colleagues[18]
376.96	EVQLVESGGGLVKPGGSLKLSCEASRFTFSSYAMSWVRQTPEKRLEWVAAISGGGRYTYYPDSMKGRFTISRDNAKN-FLYLQMSSLRSEDTAMYYCARHYDGYLDYWGQGTTLTVSSGGGGSGGGGSGGGGSDIVMTQSHKFMSTSIGARVSITCK-ASQDVRTAVAWYQQKPGQSPKLLIYSASYR-YTGVPDRFTGSGSGTDFTFTISSVQAEDLAVYYCQQHYGTPPWTFGGGTKLEI-KAAAADPTTTPAPRPPTPAPTIASQPLSLRPEACRPAAGGAVHTRGLDFACDIYIWA-PLAGTCGVLLLSLVITLYRTRSKRSRLLHSDYMNMTPRRPGPTRKHYQPYAPPRDFAAYRSRVKFSRSADAPAYQQGQNQLY-NELNLGRREEYDVLDKRRGRDPEMGGKPRRKNPQEGLYNELQKDKMAEAYSEIGMKGERRRGKGHDGLYQGLSTATKDTYDALHMQALPPR*	University of North Carolina at Chapel Hill, General Hospital Corp Patent "US10233226B2"[36]; development described by Imai[19] and ref. [37]
TE9	QVQLQQSGAALVKPGTSVKLSCK-ASGYTFTSYWMHWVKQRPGQGLEWIGMIHPKSGSVDYNEKFTNKATLTGDKSSGTAYMQLSSLTSEDSAVYY-CARGGYGSPFDYWGQGTTVTVSSGGGGSGGGGSGGGGSENVLTQSPAIMSASPGEKVTMTCSASSSVSYMY-WYQQKPGSSPRLLIYRTSNLASGVPARFSGSGSGTSYSLTISSMEAEDAA-TYYCQQWSSNPPTFGGGTKLEIKRAAADPTTTPAPRPPTPAPTIASQPLSLRPEACRPAAGGAVHTRGLDFACDIYIWA-PLAGTCGVLLLSLVITLYRTRSKRSRLLHSDYMNMTPRRPGPTRKHYQPYAPPRDFAAYRSRVKFSRSADAPAYQQGQNQLY-NELNLGRREEYDVLDKRRGRDPEMGGKPRRKNPQEGLYNELQKDKMAEAYSEIGMKGERRRGKGHDGLYQGLSTATKDTYDALHMQALPPR*	Developed in-house at UCL. Development described by ref. [20]

For the Med8A in vivo study, two types of models were run: the "high-stress" model and the 'low-stress' model. In both models, 5×10^4 Med8A cells re-suspended in PBS were injected into the cerebellum of an NSG mouse. In the "low-stress model" (illustrated in Fig. 1b), 2 days after tumor engraftment, the mice were administered intraventricularly with 2.5×10^6 CAR-T cells. In the "high-stress model" (illustrated in Fig. 1c), the mice were treated 6 days after tumor engraftment with 0.5×10^6 CAR-T cells per animal. Mice were given 200 uL luciferin (Thermo Fisher Scientific) into the scruff and imaged using a PhotonIMAGERTM optical imaging system (Biospace Lab) weekly. Animal sacrifice was initiated upon reaching either a tumor luminescence of 10E10 photons/s/cm² (via IVIS), or the appearance of tumor burden toxicity that exceeds animal welfare standards (>15% weight loss, doming of the cranium, change in activity, ataxia, dehydration, loss of normal gait, grimacing).

Tumors were dissected from humanely culled mice and dissociated into a single-cell suspension for flow cytometry analysis. They were manually cut into small pieces using a scalpel, then disaggregated with Accumax and placed on a roller for 10 min and further mashed through a 70-um cell strainer. ACK lysis buffer was used to remove red blood cells. Tumor cells were added to FACs tubes and stained according to the manufacturer's instructions. Fc receptor block was added for 10 min prior to antibody staining, then the live/dead stain and antibody mastermix was added for 20 min at 4 °C. Samples were fixed with fixation buffer (BioLegend). For panels with intracellular antibodies, BD perm/wash buffer manufacturer's instructions were followed, and intracellular antibody was added and incubated for 20 min at 4 °C. All fixed samples were run on a Symphony flow cytometer within 3 days post fixation, and analysis was done using FlowJo.

For the SUPT1 B7H3 in vivo study, NSG mice were injected with 1×10^6 SUPT1-B7H3range GFP/Luc in PBS intravenously into the tail vein. CAR-T cells (1×10^7) were injected intravenously into the tail vein at day 9 following tumor engraftment. Mice were given 200 uL luciferin (AbCam) into the scruff and imaged using a PhotonIMAGERTM optical imaging system (Biospace Lab) twice weekly. The femurs were dissected from humanely culled mice and flushed with PBS to expel bone marrow. Cell suspension was pushed through a 70-um cell strainer, and ACK lysis buffer was used to remove red blood cells. Tumor cells were added to FACs tubes and stained. Live/Dead stain was added and washed, then antibody mastermix containing Fc receptor block was

added for 30 min at 4 °C. Samples were analysed on the same day, and analysis was performed using FlowJo software.

CAR-T in vitro functional assays
A number of different functional CAR-T assays were performed. While high (>60%) transduction efficiency of CAR-T was routinely achieved, transduced cell numbers were normalized for functional assays to ensure that each binder condition receives the same number of viable CAR-T cells. All data were collected in experimental duplicates or triplicates, as indicated in the figure legends.

CAR-T responses against LAN-1 and Kelly target cells were assessed as follows. For the overnight (-18 h) co-culture cytokine assays, CAR-T cells were co-cultured with LAN-1, Kelly cells or no antigen stimulus in 48-well plates at an E:T ratio of 1:1. After 18 h, supernatant was removed for ELISA and cells were incubated with monensin (BioLegend). Checkpoint receptors PD-1, TIM-3 and LAG-3 were detected by flow cytometry. Overnight cytotoxicity was tested using a ⁵¹Cr release assay. Target cells were incubated with ⁵¹Cr for 1 h, then washed and plated in 96-well plates. CAR-T cells or untransduced cells were plated at a range of E:T ratios. The plates were incubated for 4 h at 37 °C and then the supernatant was removed and incubated with scintillation fluid (PerkinElmer) overnight at room temperature. ⁵¹Cr released into the supernatant was measured using a 1450 MicroBeta TriLux (PerkinElmer). For the re-challenge assays, CAR-T cells were co-cultured with irradiated LAN-1, Kelly, or no target cells in 24-well plates at an E:T ratio of 2:1. Cell medium was replenished every 2–3 days. CAR-T cells were challenged with irradiated target cells every 6 days, cultured for a further 24 h, and analyzed. Cells were pelleted, and supernatant was removed every week for ELISA. CAR-T cell proliferation was measured weekly by flow cytometry using Precision Count Beads (BioLegend). The levels of cytokines IL-2 and IFN-γ were quantified using ELISA MAX Deluxe Set Human IL-2 and ELISA MAX Deluxe Set Human IFN-γ (BioLegend).

SupT1-B7H3range re-challenge assays were performed as follows (illustrated in Fig. 6c). For the overnight (-18 h) co-culture cytokine assays, CAR-T cells were co-cultured with GFP/Luc-SupT1-B7H3range cells or GFP/Luc-SupT1-WT cells in 96-well plates at an E:T ratio of 1:1. After 18 h, supernatant was removed for analysis with ELISA MAX Deluxe Set Human IL-2 and ELISA MAX Deluxe Set Human IFN-γ (BioLegend). Cytotoxicity at the various indicated timepoints was tested using a luciferase-based assay. Briefly, 15 ug/mL of D-luciferin (Perkin

Elmer) was added to each well to document the remaining number of living tumor cells. The plate was then incubated for 5 min at 37 °C in 5% CO_2 and run on a SpectraMax, Molecular Devices analyzer, with "no effector" tumor wells as controls for T cell-mediated tumor death. CAR-T cells or untransduced cells were plated at a 1:1 E:T ratio, with daily re-challenges. Cytotoxicity readings were done in this manner, 18 h after each new tumor re-stimulation. CAR-T cell proliferation was measured weekly by flow cytometry using Precision Count Beads (BioLegend).

Brain tumor challenge assays with GFP/Luc-Med8A, -D425, and -D283 cells were done by plating CAR-T cells with targets at the indicated E:T ratios in 96-well plates. Cytotoxicity at 96 h following tumor challenge was tested using a luciferase-based assay. Briefly, 15 ug/mL of D-luciferin (Perkin Elmer) was added to each well to document the remaining number of living tumor cells. The plate was then incubated for 5 min at 37 °C in 5% CO_2 and run on a SpectraMax, Molecular Devices analyzer, with "no effector" tumor wells as controls for T cell-mediated tumor death. CAR-T cell proliferation was measured weekly by flow cytometry using Precision Count Beads (BioLegend).

Malignant rhabdoid tumoroids were established, characterized and cultured as previously described[31,32]. 103-T tumoroids were transduced with a construct encoding for luciferase were cultured in KOM in BME droplets for 7 days in advance. Four days before the co-culture, the tumoroids were disrupted mechanically into a single cell suspension by mechanical dissociation and seeded in BME droplets. On the day of the CAR-T challenge, MRT tumoroids were collected, washed with cold medium to remove BME, and a fraction was dissociated into a single cell suspension. Single tumor cells were counted to determine the number of cells present in the MRT tumoroid suspension. MRT tumoroids were then seeded out with an equivalent of 7500 single tumor cells per well in 50 uL of co-culture medium containing 10% FBS and a 1:1 ratio of KOM and RPMI with 1X GlutaMAX and 1X P/S. To determine tumor-specific killing, a released luciferase assay was performed using the luciferase assay system (Promega). Medium was removed and cells were washed with 100 uL of PBS. 20 uL of 1X passive lysis buffer (Promega) were added and the plate was incubated at room temperature for 15 min while shaking. In a LUMITRAC white polystyrene 96-well plate (Greiner) 100 uL of the luciferase reagent were added to 20 uL of the lysed cells and the plate was measured at the FluoSTAR Omega Microplate reader immediately. Luciferase signal was determined on day 1 after co-culture, as well as before re-challenge with new tumoroids.

To measure CAR-T cytotoxicity against (AMC) 691-B and 691-T neuroblastoma tumoroids, GFP-Luc tumoroids were dissociated into single cells by resuspending in 1 mL of Accutase solution (Sigma-Aldrich) through a p10 tip on top of a p1000 tip to combine both enzymatic and mechanical dissociation methods. Tumoroid cells in suspension were counted and plated two days before the beginning of the experiment to ensure spheroid formation in 96-well white flat-bottom plates (Costar). On the day of initiation, co-culture, CAR-T cells were counted and plated with GFP/Luc tumoroids at the stated E:T ratios in half "neurosphere medium" (expanded on in the Cell Lines section of Methods and Materials) and half T cell medium (RPMI-GlutaMAX 1640 + 25 mM Hepes (Thermo Fisher) supplemented with 10% FCS (Gibco), 1% penicillin/streptomycin (Thermo Fisher), and 1% L-glutamine (Thermo Fisher) supplemented with 100 IU/mL IL-2 (Miltenyi Biotec). For re-challenge, tumoroids were plated 2 days before each challenge, with the CAR-T culture added on top. Tumoroid re-challenge with a set E:T ratio was done every 2–3 days. Cytotoxicity was measured by adding 15 ug/mL of D-luciferin (Perkin Elmer) to each well to document the remaining number of living tumor cells, with "no effector" tumor wells as controls for T cell-mediated tumor death. Cells were then incubated for 5' at 37 °C in 5% CO_2 and readout performed in the FLUOstar Omega microplate reader.

Flow cytometry staining and analysis

The following cell cytometers were used to collect flow cytometry data: BD® LSR II Flow Cytometer (BD Biosciences), FACSymphony™ A5 High-Parameter Cell Analyzer (BD Biosciences) and CytoFLEX S V4-B2-Y4-R3 Flow Cytometer (Beckman Coulter). FlowJo 10.9.0 software for Mac (Becton Dickinson) was used to analyse flow cytometry data. All staining was done in FACS buffer, PBS, 2% FCS with 2 mM EDTA. Samples were either analysed immediately following staining or fixed with Biolegend Fixation Buffer and analysed within two weeks. The following Table 3 lists the flow cytometry staining reagents that were used:

Lumicks CAR-T avidity measurements

Proprietary z-Movi Lumicks protocols were followed. Briefly, SupT1-WT, SupT1-B7H3hi, LAN-1, and Med8A tumor cells were seeded in a z-Movi microfluidic chip (Lumicks, Amsterdam, Netherlands) coated with poly-L-lysine and cultured for 16 h. The next day, flow sorted, transduction efficiency-normalized and CellTrace Red (BioLegend)-labeled CAR-T cells of greater than 90% viability were serially flowed in the chips and incubated with the target cells for 10 min prior to initializing a 3-min linear force ramp (deviation from protocol standard of 2.5 min). During the force ramp, the z-Movi device (Lumicks) captured a time series of images using a bright field microscope integrated into the platform. Detached cells were levitated towards the acoustic nodes, allowing the tracking of cells based on their XY positions. Changes in the Z-position resulted in a change in the diffraction pattern, which allowed the distinction between cells adhered to the substrate and cells suspended over the acoustic nodes. This information was used to correlate cell detachment events with a specific rupture force. Cell detachment was acquired using z-Movi Tracking, and post experiment image analysis was done using Cell Tracking offline analysis. Data were presented as "mean % CAR-T attached cells" at the maximum mean force applied, 1000 piconewtons, pN. This was repeated in experimental triplicate (different chips for the same experiment) for four biological T cell donors. A greater depth of the z-Movi workflow is reported online[38]. The software used to acquire the data was z-Movi Software (v1.0).

Binder affinity measurements

Biacore surface plasmon resonance (SPR) for anti-B7H3 antibodies was done as previously described[39]. Briefly, MGA271, 376.96, and TE9 binders were expressed in human IgG1 format (Evitria), and then evaluated by Antibody Analytics using Biacore SPR for binding kinetics to 4-Ig human B7H3. Anti-B7H3 antibodies were first adhered to plates, and several concentrations of Human B7H3 analyte were passed over the surface to assess the binding interactions. Clone 9G8 mAb was used as an isotype control.

BEHAV3D CAR-T/tumoroid imaging

Tumoroids (691-B and -T) were grown in "Neurosphere medium" (as described in the "Cell Lines" section), cultured for 3 weeks prior to the experiments and passaged once or twice a week according to tumoroid size and confluence. The experimental timeline is illustrated in Fig. 7a. CAR-T cells were thawed one day prior to the start of the experiment in RPMI-GlutaMAX 1640 + 25 mM Hepes (Thermo Fisher) supplemented with 10% FCS (Gibco), 1% penicillin/streptomycin (Thermo Fisher) and 1% L-glutamine (Thermo Fisher), rested overnight at a density of 1×10^7 cells/mL in 100 IU/mL IL-2 (Miltenyi Biotec)-supplemented medium. CAR-T cells for the initial challenge day 0 imaging experiment were stained with the following antibody mix in FACS buffer (PBS 1x + 2% FCS + 2 mM EDTA): anti-RQR8 mAb clone QBEND10-APC (R&D Systems), anti-CD4 mAb clone VIT4-VioBlue (Miltenyi Biotec) and mouse serum (Invitrogen). RQR8+CD4+ and

Table 3 | List of antibodies used in the study

Target	Product ID	Catalog Number
Viability dye	Fixable Blue Dead Cell Stain — LIVE/Dead™ (Thermo)	L34961
Flow count beads	Precision Count Beads (Biolegend)	424902
B7H3-his	B7H3-his protein to detect CAR at the cell surface (R&D Biosystems)	1949-B3-050/CF
His	Anti-his mAb clone J095G46-APC (BioLegend)	362605
Ag density quantification	BD Biosciences™ Quantibrite™ Phycoerythrin (PE) Beads; used to quantify B7H3 antigen density on target cell surface	10626384
Fixation buffer	Fixation buffer (Biolegend)	420801
Cell membrane dye	eBioscience Cell Proliferation Dye eFluor 450 (blue) (Thermo Fisher); used to label cells for BEHAV3D analysis	65-0842-85
Cell membrane dye	Calcein AM (green) (Thermo Fisher); used to label cells for BEHAV3D analysis	C1430
Cell membrane dye	CellTrace™ Far Red Cell Proliferation Kit, for flow cytometry; used to label cells for Lumicks z-Movi analysis	C34564
RQR8 marker gene	Clone QBEND10-APC (BioTechne)	FAB7227A
CD3	Clone OKT-3-Brilliant Violet 711 (Biolegend)	317328
CD4	Clone VIT4-VioBlue (Miltenyi Biotec),	130-113-219
B7H3	Clone MIH42-PE (BioLegend)	351003
PD-1	Clone EH12.1-Brilliant Violet 605 (Beckton Dickinson)	563245
CD25	Clone 2A3-Briljant Violet 711 (Beckton Dickinson)	563159
CD4	Clone A161A1-FITC (BioLegend)	357406
CD8	Clone SK1-PerCP (BioLegend)	344706
TIM-3	Clone F38-2E2-PE (BioLegend)	345006
CCR7	Clone G043H7-PE/Dazzle594 (BioLegend)	353235
CD69	Clone FN50-PE-Cy7 (Beckton Dickinson)	561928
CD137	Clone 4B4-1-APC (Beckton Dickinson)	550890
CD3	Clone HIT3a-Alexa Fluor 700 (BioLegend)	300324
muCD45	Clone 30-F11-APC/Fire™ 810 (BioLegend)	103173
CD45RA	Clone HI100-APC/Cy7 (Beckton Dickinson)	750258

RQR8$^+$CD4$^-$ CAR-T cells were FACS-sorted with a Sony SH800S cell sorter into FCS, and rested overnight at a density of 1×10^7 cells/mL in medium supplemented with 100 IU/mL IL-2 (Miltenyi Biotec).

For co-culture experiments, tumoroids were dissociated into single cells by pipetting 1 mL of Accutase solution (Sigma-Aldrich, counted and plated 2 days before the beginning of the experiment to ensure spheroid formation in either 12-well flat-bottom plates (for re-challenges) (Greiner) or in a glass-bottom 96-well SensoPlate (Greiner) for imaging. The correct cell number was determined considering organoid growth rates. Wild-type organoids were used. Sorted and rested CAR-T cells were stained separately with eBioscience Cell Proliferation Dye eFluor 450 (1:4000, Thermo Fisher) or Calcein AM (1:3000, Thermo Fisher) in PBS for 15 min at 37 °C and mixed in a 1:1 ratio immediately before plating them with the organoids in a 1:5 E:T ratio. The co-culture medium (100 µL organoids + 100 µL T cells) was then supplemented with 2.5% basement membrane extract (BME, Cultrex), Nucred Dead 647 (three drops per mL, Thermo Fisher), and TO-PRO-3 (1:5000, Thermo Fisher). The combination of Nucred Dead 647 and TO-PRO-3 has previously been described by ref. 25. The plate was placed in a SP8 confocal microscope (Leica) containing an incubation chamber (37 °C, 5% CO$_2$) and imaged for 13 h in time series with 2-min intervals (as shown in Supplementary Fig. 10). Day 7 BEHAV3D imaging was the third challenge with 691 tumoroids. On Day 6, cells from re-challenge plates were stained with the following antibody mix in FACS buffer (PBS1x + 2% FCS + 2 mM EDTA): anti-RQR8 mAb clone QBEND10-APC (R&D Systems), anti-CD4 mAb clone VIT4-VioBlue (Miltenyi Biotec), anti-B7H3 mAb clone MIH42-PE (BioLegend) and mouse serum (Invitrogen). B7H3$^-$ CD34$^+$CD4$^+$ and B7H3$^-$ CD34$^+$CD4$^-$ CAR-T cells were FACS-sorted with the Sony SH800S cell sorter into FCS, rested overnight at a density of 1×10^7 cells/mL in medium supplemented with 100 IU/mL IL-2 (Miltenyi Biotec). On day 7, rested CAR-T cells were stained separately and plated with WT organoids in a 1:5

E:T ratio, as described above. The plate was placed in a SP8 confocal microscope (Leica) containing an incubation chamber (37 °C, 5% CO$_2$) and imaged for 13 h in time series with a 2-min interval.

Image processing was done according to the protocol previously described by ref. 25 using the Imaris (Oxford Instruments) version 10.0 software for 3D visualization, cell segmentation and extraction of statistics. The Channel Arithmetics Xtension was used to create additional channels for the specific identification of CD8$^+$ and CD4$^+$ T cells (live and dead), organoids (live and dead), and to exclude debris. The Surface and ImarisTrack modules were used to specifically detect and track T cells and/or organoids. For tracked T cells, time-lapse statistics consisting of the coordinates of each cell, speed, square displacement, distance to either organoids or the other T cell subset, and dead cell dye channel intensity were exported into a metadata file for subsequent processing and analysis. Full protocols for BEHAV3D analysis are recently published[38] and script for data analysis are publically available at https://github.com/AlievaRios/BEHAV3D.

Data presentation
Data were graphed and analysed statistically using Graphpad Prism 10 for macOS software (Dotmatics). Statistical tests were chosen as suitable to particular data sets, and statistical test recommendations by Graphpad Prism 10 software were followed, based on data type, replicates and degree of pairing. The number of biological and experimental replicates used in each analysis is listed in the respective figure legends. Data processing for the BEHAV3D platform was done using the "R" programming language code that was written by and published by the Rios group[31].

Reporting summary
Further information on research design is available in the Nature Portfolio Reporting Summary linked to this article.

Data availability

Raw data are available in the article and its Supplementary files or from the corresponding author upon request. Source data are provided with this paper.

References

1. Albelda, S. M. CAR T cell therapy for patients with solid tumours: key lessons to learn and unlearn. *Nat. Rev. Clin. Oncol.* **21**, 47–66 (2024).
2. Majzner, R. G. & Mackall, C. L. Tumor antigen escape from CAR T-cell therapy. *Cancer Discov.* **8**, 1219–1226 (2018).
3. Labanieh, L. & Mackall, C. L. CAR immune cells: design principles, resistance and the next generation. *Nature* **614**, 635–648 (2023).
4. Weber, E. W. et al. Transient rest restores functionality in exhausted CAR-T cells through epigenetic remodeling. *Science* **372**, eaba1786 (2021).
5. Weber, E. W. et al. Pharmacologic control of CAR-T cell function using dasatinib. *Blood Adv.* **3**, 711–717 (2019).
6. Ghorashian, S. et al. Enhanced CAR T cell expansion and prolonged persistence in pediatric patients with ALL treated with a low-affinity CD19 CAR. *Nat. Med.* **25**, 1408–1414 (2019).
7. Majzner, R. G. et al. Tuning the antigen density requirement for CAR T-cell activity. *Cancer Discov.* **10**, 702–723 (2020).
8. Du, H. et al. Antitumor responses in the absence of toxicity in solid tumors by targeting B7-H3 via chimeric antigen receptor T cells. *Cancer Cell* **35**, 221–237.e8 (2019).
9. Theruvath, J. et al. Locoregionally administered B7-H3-targeted CAR T cells for treatment of atypical teratoid/rhabdoid tumors. *Nat. Med.* **26**, 712–719 (2020).
10. Majzner, R. G. et al. CAR T cells targeting B7-H3, a Pan-cancer antigen, demonstrate potent preclinical activity against pediatric solid tumors and brain tumors. *Clin. Cancer Res.* **25**, 2560–2574 (2019).
11. Maachani, U. B. et al. B7-H3 as a prognostic biomarker and therapeutic target in pediatric central nervous system tumors. *Transl. Oncol.* **13**, 365–371 (2019).
12. Modak, S., Kramer, K., Gultekin, S. H., Guo, H.-F. & Cheung, N. K. Monoclonal antibody 8H9 targets a novel cell surface antigen expressed by a wide spectrum of human solid tumors. *Cancer Res.* **61**, 4048–4054 (2001).
13. Chapoval, A. I. et al. B7-H3: A costimulatory molecule for T cell activation and IFN-γ production. *Nat. Immunol.* **2**, 269–274 (2001).
14. Wang, L., Kang, F.-B. & Shan, B.-E. B7-H3-mediated tumor immunology: friend or foe?. *Int. J. Cancer* **134**, 2764–2771 (2014).
15. Vitanza, N. A. et al. Intraventricular B7-H3 CAR T cells for diffuse intrinsic pontine glioma: preliminary first-in-human bioactivity and safety. *Cancer Discov.* **13**, 114–131 (2022).
16. Leick, M. B. et al. Non-cleavable hinge enhances avidity and expansion of CAR-T cells for acute myeloid leukemia. *Cancer Cell* **40**, 494–508.e5 (2022).
17. Salzer, B. et al. Engineering AvidCARs for combinatorial antigen recognition and reversible control of CAR function. *Nat. Commun.* **11**, 4166 (2020).
18. Han, C. et al. Desensitized chimeric antigen receptor T cells selectively recognize target cells with enhanced antigen expression. *Nat. Commun.* **9**, 468 (2018).
19. Chmielewski, M., Hombach, A., Heuser, C., Adams, G. P. & Abken, H. T cell activation by antibody-like immunoreceptors: increase in affinity of the single-chain fragment domain above threshold does not increase T cell activation against antigen-positive target cells but decreases selectivity. *J. Immunol.* **173**, 7647–7653 (2004).
20. Mause, E. R. V. et al. Systematic single amino acid affinity tuning of CD229 CAR T cells retains efficacy against multiple myeloma and

21. Olson, M. L. et al. Low-affinity CAR T cells exhibit reduced trogocytosis, preventing rapid antigen loss, and increasing CAR T cell expansion. *Leukemia* **36**, 1943–1946 (2022).
22. Greenman, R. et al. Shaping functional avidity of CAR T cells: affinity, avidity, and antigen density that regulate response. *Mol. Cancer Ther.* **20**, 872–884 (2021).
23. Loo, D. et al. Development of an Fc-enhanced anti-B7-H3 monoclonal antibody with potent antitumor activity. *Clin. Cancer Res.* **18**, 3834–3845 (2012).
24. Imai, K., Wilson, B. S., Bigotti, A., Natali, P. G. & Ferrone, S. A 94,000-dalton glycoprotein expressed by human melanoma and carcinoma cells. *J. Natl Cancer Inst.* **68**, 761–769 (1982).
25. Birley, K. et al. A novel anti-B7-H3 chimeric antigen receptor from a single-chain antibody library for immunotherapy of solid cancers. *Mol. Ther. Oncolytics* **26**, 429–443 (2022).
26. Lamers, C. H. J. et al. Phoenix-ampho outperforms PG13 as retroviral packaging cells to transduce human T cells with tumor-specific receptors: implications for clinical immunogene therapy of cancer. *Cancer Gene Ther.* **13**, 503–509 (2006).
27. Philip, B. et al. A highly compact epitope-based marker/suicide gene for easier and safer T-cell therapy. *Blood* **124**, 1277–1287 (2014).
28. Nguyen, P. et al. Route of 41BB/41BBL costimulation determines effector function of B7-H3-CAR.CD28ζ T cells. *Mol. Ther. Oncolytics* **18**, 202–214 (2020).
29. Labanieh, L. et al. Enhanced safety and efficacy of protease-regulated CAR-T cell receptors. *Cell* **185**, 1745–1763.e22 (2022).
30. Orlova, D. Y. et al. Earth mover's distance (EMD): a true metric for comparing biomarker expression levels in cell populations. *PLos ONE* **11**, e0151859 (2016).
31. Dekkers, J. F. et al. Uncovering the mode of action of engineered T cells in patient cancer organoids. *Nat. Biotechnol.* **41**, 60–69 (2022).
32. Sajman, J. et al. Nanoscale CAR organization at the immune synapse correlates with CAR-T effector functions. *Cells* **12**, 2261 (2023).
33. Xiong, Y., Libby, K. A. & Su, X. The physical landscape of CAR-T synapse. *Biophys. J.* **123**, 2199–2210 (2024).
34. Halim, L. et al. Engineering of an avidity-optimized CD19-specific parallel chimeric antigen receptor that delivers dual CD28 and 4-1BB co-stimulation. *Front. Immunol.* **13**, 836549 (2022).
35. Kontos, F. et al. B7-H3: an attractive target for antibody-based immunotherapy. *Clin. Cancer Res.* **27**, 1227–1235 (2020).
36. Zhou, W.-T. & Jin, W.-L. B7-H3/CD276: an emerging cancer immunotherapy. *Front. Immunol.* **12**, 701006 (2021).
37. Seaman, S. et al. Eradication of tumors through simultaneous ablation of CD276/B7-H3-positive tumor cells and tumor vasculature. *Cancer Cell* **31**, 501–515.e8 (2017).
38. Alieva, M. et al. BEHAV3D: a 3D live imaging platform for comprehensive analysis of engineered T cell behavior and tumor response. *Nat. Protoc.* **19**, 2052–2084 (2024).
39. Jason-Moller, L., Murphy, M. & Bruno, J. Overview of Biacore systems and their applications. *Curr Protoc Protein Sci.* Ch. 19, Unit 19.13 https://doi.org/10.1002/0471140864.ps1913s45 (2006).

Author contributions

MBa, J.W., and J.A. wrote the manuscript; M.Ba, H.M., E.Z., M.B.R., J.F., and S.d.B. analyzed data; G.F. generated reagents; E.Z., H.M., I.A., R.S., B.D., C.H., C.B., S.M.T., M.N., S.M., K.B., C.L.B., A.V., L.P., K.O.S., A.G., R.N., D.S., F.v.d.H., B.v.V., G.F., and M.Bu performed experiments; J.A., J.W., J.B., K.C., A.R., J.D., J.M., L.C., P.S., L.D., and R.R. co-supervised the research: J.A., P.S., L.C., J.W., J.M., A.R., J.D., S.G. provided grant support.

Competing interests

Additional information

Correspondence and requests for materials should be addressed to Marta Barisa, Judith Wienke or John Anderson.

[1]Great Ormond Street Institute of Child Health, University College London, London, UK. [2]Princess Máxima Center for Pediatric Oncology, Utrecht, The Netherlands. [3]Oncode Institute, Utrecht, The Netherlands. [4]Lumicks, Amsterdam, The Netherlands. [5]Department of Pediatrics, University of Wisconsin School of Medicine and Public Health, University of Wisconsin-Madison, Madison, WI, USA. [6]Cancer Institute, University College London, London, UK. [7]The Institute of Cancer Research, London, UK. [8]These authors contributed equally: Henrike P. Muller, Elisa Zappa. ✉e-mail: m.barisa@ucl.ac.uk; j.wienke-4@prinses-maximacentrum.nl; j.anderson@ucl.ac.uk